Project No. 10-69

Guidelines for Dowel Alignment in Concrete Pavements

APPENDIX D
FINITE ELEMENT ANALYSIS

Prepared for
NATIONAL COOPERATIVE HIGHWAY RESEARCH PROGRAM (NCHRP)
Transportation Research Board
of
The National Academies

Priyam Saxena, Research Assistant
University of Minnesota
Alex Gotlif, Staff Engineer
Applied Research Associates, Inc.
Lev Khazanovich, Ph.D., Associate Professor
University of Minnesota

Minneapolis, MN
February 2009

APPENDIX D. FINITE ELEMENT ANALYSIS

D.1 INTRODUCTION

This appendix presents a detailed description of the 3D finite element models described in sections 2.3.3.1 and 3.3 of the main report. The following two 3D ABAQUS models were developed in this study to provide detailed modeling of the dowel-concrete interaction under various types of misalignments.

- Beam models with individual dowels
- Slab models with four dowels

The beam model simulates the laboratory beam test of individual dowels conducted in this study and described in Appendix C. The model was calibrated using the results of the laboratory testing and was used to run extended misalignment cases and magnitudes that were not tested in the lab. The slab model permits an analysis of the effect of multiple dowel misalignment on behavior of a joint in a concrete pavement subjected to concrete slab contraction and expansion as well as axle loading.

D.2 BEAM MODEL

The beam finite element model was used to simulate both modified pullout and shear pull laboratory tests. In the lab, shear testing was conducted after the pullout testing to model the effect of joint opening prior to wheel loading. In a similar manner, the finite element beam model was set up to apply the pullout test prior to applying the shear pull test, thus anticipating any damage accumulated in the concrete beam. The beam model is shown in Figure D.1. It contains 8700 eight-node, reduced-integration 3D linear brick elements of type C3D8R. Multiple parts were used to assemble the model. This includes the concrete, the dowel, and all the clamping fixtures and base.

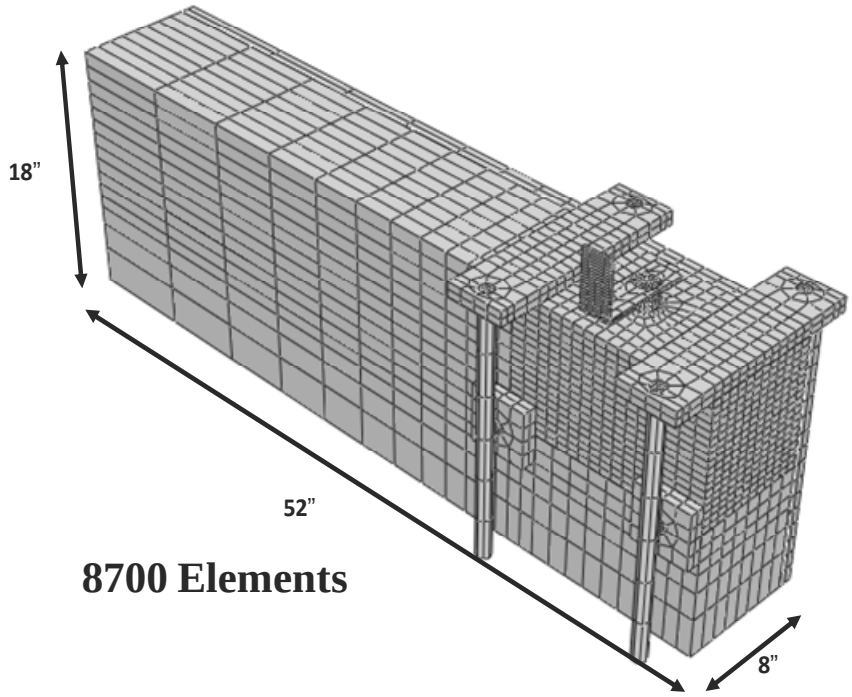

Figure D.1. The beam model structure.

D.2.1 Parts and Material Properties

The beam model consisted of ten 3D deformable parts, shown in Figure D.2. Three parts formed the concrete section, one part the dowel, one part the angle, two parts formed the pullout load clamping fixture, and the rest three parts formed the shear load clamping fixture. ABAQUS lets the user define exact replicas of the parts, called "instances." Multiple instances of the same part could be used to assemble the model, thereby reducing the time and effort to model the part over and over again.

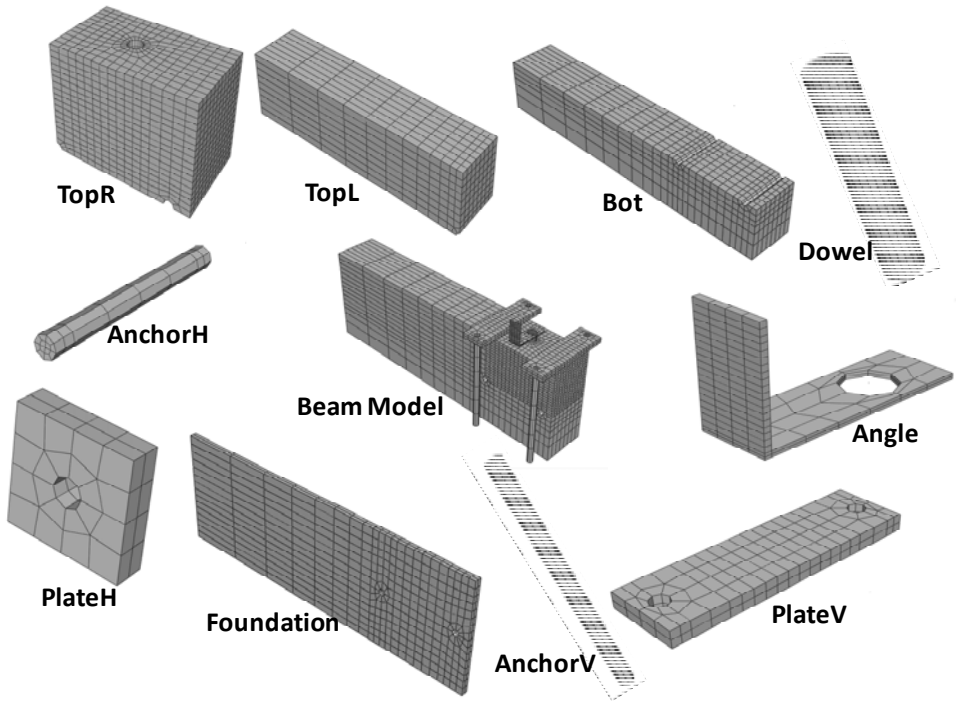

Figure D.2. Parts of the beam model (parts are not scaled according to actual size).

D.2.1.1 The Concrete Section of the Beam Model

The concrete section was divided into top right, top left, and bottom parts. The top right part has a quarter circular and a semicircular cut, and the top left part has a quarter circular cut on their lower surfaces, to go over the horizontal anchors used in the shear load fixture. Similarly, the bottom part has two semicircular cuts on its top surface to go below the horizontal anchors. The horizontal anchors go through these holes and tie the horizontal plates to the base plate.

1. TopR (top right part) – This part represents the concrete around the dowel. The solid extrude has a dimension of 14 x 9 x 8 in.. It has two cuts, one quarter-circular at the bottom left edge and a semicircular cut with center at 2 in. from the bottom right edge. Both the cuts have a radius of 0.5 in. The central cut extrude has a diameter of 1.5 in. (equal to the diameter of the dowel), and it is a blind cut 9 in. deep. It is drawn using two datum points, a datum axis, and a datum plane. One instance of this part has been used in the assembly.

   The mesh has 3780 elements. As the response of the concrete was of high interest in this part, a finer mesh was assigned to it. Although more computational time was needed for the finer mesh, the higher mesh density allowed for more accurate analysis of the strains, stresses, and deflections at the most relevant points.

   The material property defined for this part was named “Concrete.” It was modeled using the using the concrete damaged plasticity option available in ABAQUS. The inelastic behavior of concrete was modeled using the concept of isotropic damaged

elasticity in combination with isotropic tensile and compressive plasticity (ABAQUS, 2007; Lee and Fenves, 1998; Lubliner 1989). It accounts for the loss of elastic stiffness due to plastic straining in tension and compression. The dilation angle was taken as 30° while all the other parameters—eccentricity (= 0.1), equibiaxial to uniaxial compressive stress ratio (= 1.16), ratio of the second stress invariant on the tensile to compressive meridian (= 0.667), and viscosity parameter (= 0)—were taken as ABAQUS defaults. The Poisson's ratio and the coefficient of thermal expansion were assigned to be equal to 0.2 and 5E-06, respectively.

The compressive strength f_c' of 5000 psi was selected based on the results of laboratory testing. From the compressive strength, the initial yield strength in elastic range f_{ce} was estimated to be 3500 psi, the direct tensile strength f_t was estimated to be 350 psi, and the modulus of elasticity E was estimated as 4030 ksi using the following relations (Mindess et al., 2003):

$$f_{ce} = 0.7 f_c', \quad f_t = 0.09 f_t', \quad \text{and} \quad E = 57000\sqrt{f_c'}$$

2. TopL (top left part) – This part represents the upper left part of the concrete beam that does not contain the dowel. The solid extrude has a dimension of 38 x 9 x 8 in. A quarter-circular cut of radius 0.5 in. is present at the bottom right edge of the part. One instance of this part has been used in the assembly. The mesh has 872 elements. It was denser towards the TopR part, while large element sizes were assigned away from the dowel. The material property assigned to this part was "Concrete," as with TopR.

3. Bot (bottom part) – This part represents the bottom part of the concrete beam. The solid extrude has a dimension of 52 x 9 x 8 in. Two semicircular cuts are present with centers at 2 in. and 14 in. from the right edge. One instance of this part was used in the assembly. The mesh has 1184 elements. The material property assigned to this part was called "Concrete2." The material "Concrete2" was used instead of "Concrete" (as above) to better model the initial assembly. The stiffness was defined as a fictional, temperature dependent property. With a change in temperature, this part was shifted from a very soft material (E = 4 ksi) to the actual stiffness E = 4,030 ksi. As this part did not contain the dowel and did not experience high stresses, an elastic analysis was sufficient for this region. This saved computational time without compromising on the accuracy of the results. The Poisson's ratio and the coefficient of thermal expansion were assigned to be 0.2 and 5E-06, respectively.

D.2.1.2 The Dowel-Angle Section

The dowel-angle section consisted of a dowel and an angle. In the laboratory test, the angle was attached to the dowel to enable the LVDT measurements during shear testing. To maintain similarity between the laboratory setup and the FE model, the angle was also kept in the beam model. Thus, the displacements could be read at the exact positions of the LVDTs as in the lab.

4. Dowel – The solid extrude has a depth of 10.5 in. and a radius of 0.75 in. The dowel is attached to the angle to measure the displacement using a LVDT. One instance of this part has been used in the assembly. The mesh has 1056 elements. The material property assigned to this part was called "Steel." It was modeled as an elastic isotropic material with modulus of elasticity, Poisson's ratio, and coefficient of thermal expansion as 29000 ksi, 0.3, and 5E-06, respectively. To model the embedment length misalignment, a new material property called "Steel2" was created. It also was modeled as an elastic isotropic material with modulus of elasticity as 1 ksi. The Poisson's ratio and the coefficient of thermal expansion were the same as for "Steel."

5. Angle – The solid extrude has a dimension of 6 x 4 x 2 in. The thickness of the part is 0.2 in. The cut extrude has a radius of 0.75 in., and it is a blind cut 0.2 in. deep. One instance of this part has been used in the assembly. The mesh has 140 elements. The material property assigned to this part was "Steel," the same material used for the Dowel.

D.2.1.3 The Pullout Test Fixture

The pullout test fixture clamped the concrete beam to the surface, while the dowel was being pulled out away from the concrete. Two vertical plates and four vertical anchors were used to simulate the pullout test fixture. The shear test constrains were simulated by a base plate, two horizontal plates, and two horizontal anchors. To simplify adding or removing the clamping mechanism when changing the simulation from pullout to shear testing, a fictitious temperature sensitive stiffness was defined for both the pullout and the shear test fixtures. Depending on the prescribed fictitious temperatures, the stiffness of each of these parts can be either very high or very low.

6. PlateV (vertical plate) – The solid extrude has a dimension of 14 x 4 x 1 in. Two circular cut extrudes were present with centers at 1 in. from the left and right edges of the part. Two instances of this part have been used in the assembly. The mesh has 176 elements. The material property defined for this section is called "PlateV." During the initial assembly and the pullout test, the stiffness was equal to 3E+10 psi, which gets reduced to 300 psi prior to shear loading. The Poisson's ratio and the coefficient of thermal expansion were assigned to be 0.3 and 5E-06, respectively.

7. AnchorV (vertical anchor) – The vertical anchors are created to simulate the supports used in the pullout test. The solid extrude has a cylindrical shape of depth of 19 in. and radius of 0.5 in.. Four instances of this part have been used in the assembly. The mesh has 96 elements. The material property assigned to this section is "PlateV."

D.2.1.4 The Shear Test Fixture

In shear test, a horizontal fixture restricted the movement of the beam, and it consisted of a base plate, two horizontal plates, and two horizontal anchors.

8. Foundation (Base Plate) – The solid extrude has a dimension of 52 x 18 x 1 in. Two circular cut extrudes are present with centers at 2 in. and 14 in. from the right edge. One instance of this part has been used in the assembly. The mesh has 660 elements. The material property defined for this section is called "Foundation." During the initial assembly and the pullout test, the stiffness was equal to 100 psi, which was increased to 1E+07 psi prior to shear loading. The Poisson's ratio and the coefficient of thermal expansion were assigned to be 0.3 and 5E-06, respectively.

9. PlateH (Horizontal Plate) – The solid extrude has a dimension of 4 x 4 x 1 in. A circular cut extrude is present at the center of the part with radius of 0.5 in. Two instances of this part have been used in the assembly. The mesh has 40 elements. The material property assigned to this section is "Foundation."

10. AnchorH (Horizontal Anchor) – The horizontal anchors are created to simulate the rods to tie the supports used in the shear test. The solid extrude has a cylindrical shape of depth of 10 in. and radius of 0.5 in.. Two instances of this part have been used in the assembly. The mesh has 96 elements. The material property defined for this section is called "AnchorH." During the initial assembly and the pullout test, the stiffness was equal to 100 psi, which was increased to 3E+08 psi prior to shear loading. The Poisson's ratio and the coefficient of thermal expansion were assigned to be 0.3 and 5E-06, respectively.

D.2.2 Contact Interactions

Two contact interactions are defined in the beam model, namely contact between the dowel and the concrete surrounding it (*dowel-concrete interaction*) and contact between the base plate and the concrete in contact with it (*foundation-concrete interaction*). Previous studies (e.g., Khazanovich et al., 2001) have shown that even though dowel coating significantly reduces friction between the dowel and the surrounding concrete, friction is not completely eliminated and, therefore, has to be considered in the analysis. The friction model in ABAQUS is an extended version of the classical Coulomb friction model (Amoton's Law), which states that the contact surfaces do not slide over each other if the shear stress magnitude is less than the coefficient of friction μ times the pressure stress between them (see Figure D.3).

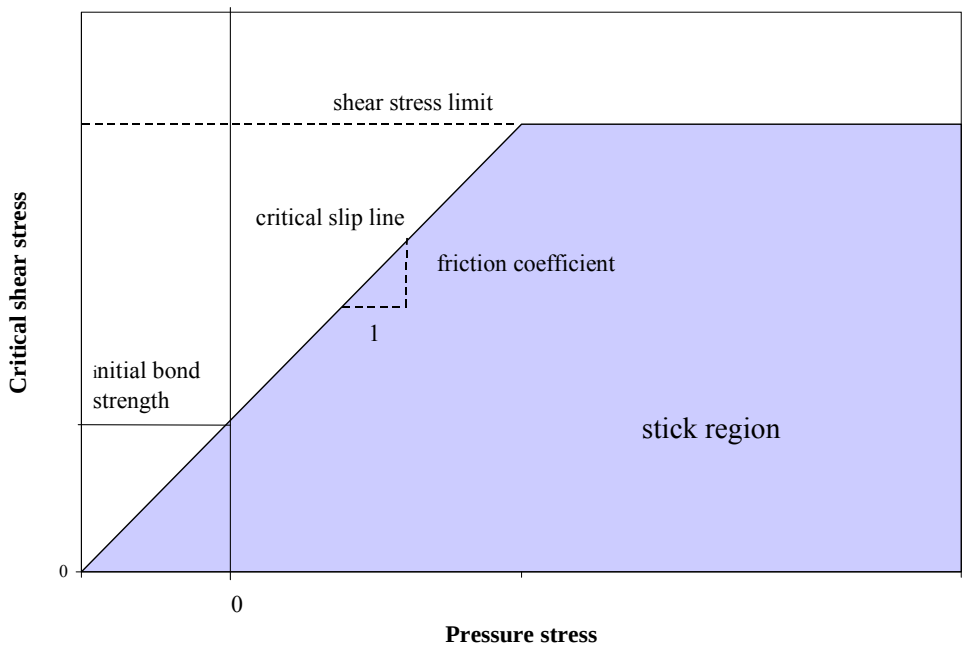

Figure D.3. Dowel/PCC contact modeling in ABAQUS (Khazanovich et al., 2001).

The dowel-concrete interaction was modeled as a surface-to-surface contact defined between two deformable bodies. Small sliding was selected to ensure that the surfaces do not slide too much along each other relatively. The internal ABAQUS parameter that governs the sliding effect, depth of the adjustment zone (ABAQUS, 2007), was specified as 0.1 in. (The adjustment zone is the area in which the nodes of the slave surface can penetrate the master surface.) The constraint enforcement method used was "node to surface." No initial clearance was specified between the dowel and the concrete around it. The frictional formulation defined is "Penalty." The friction coefficient was 0.3, and the maximum shear stress magnitude was 100 psi.

The dowel-concrete normal behavior was modeled using the ABAQUS "Hard Contact" option (ABAQUS, 2007). This option minimizes penetration of the dowel into the surrounding concrete at the contact interface and does not allow the transfer of tensile stress across the interface.

In the laboratory tests, the concrete beam was anchored to the heavy steel base plate by two thick rods. While the concrete beam was subjected to a shear pull loading, there was the possibility that the beam could separate from the base plate. In the finite element model, the base plate was modeled as the part "Foundation." A *foundation-concrete interaction* was defined between the base plate and the concrete beam to prevent the beam from penetrating into the steel plate while still allowing for separation to occur between the beam and the plate.

The foundation-concrete interaction was modeled as a surface-to-surface contact. Small sliding was selected as the sliding formulation, and the constraint enforcement method used was "node to surface" with no adjustment zone. The initial clearance specified was a uniform value of 0.01 across the slave surface. This was selected from the results of

calibration of the model, explained in section D.3.1. The contact was defined as frictionless. The normal behavior was defined as a "Hard Contact."

All other parts were tied together using "Tie" constraints. This constraint ties two separate surfaces together so that there is no relative motion between them. It allows fusing together two regions even though the meshes created on the surfaces of the regions may be dissimilar.

D.2.3 Loading

The beam model was loaded in two stages as in the laboratory. The concrete beam was first subjected to a pullout loading, which was followed by a shear pull loading. The point of application for both the loads was same.

D.2.3.1 Pullout Loading

A total load of 4020 lb was applied in the load control mode. It was ramped in 10 increments. In the displacement control mode a prescribed displacement of 0.03 in. was applied, ramped in 10 increments. The point of application is the center of the exposed dowel, in other words, the dowel between the concrete and the angle. Figure D.4 shows the pullout test model.

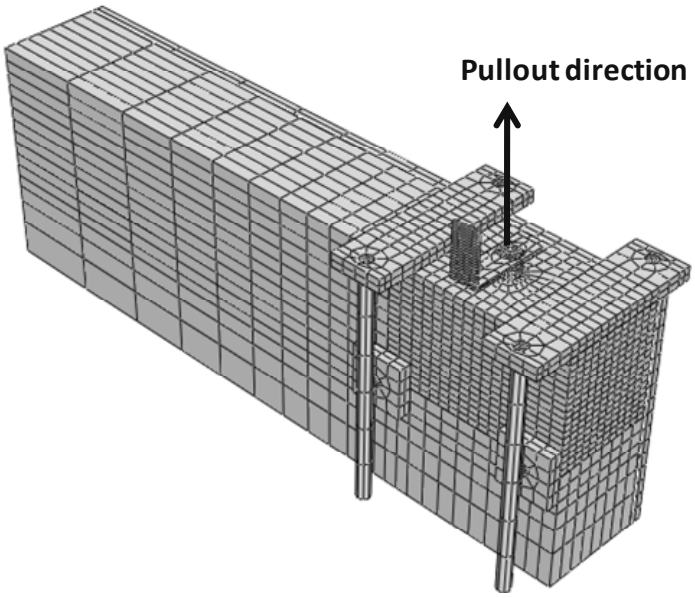

Figure D.4. The pullout loading direction.

D.2.3.2 Shear Pull Loading

When the test was changed from pullout to shear, the vertical fixture became a very soft material while the horizontal fixture became the stiffer material. A total load of 8000 lb was applied in the load control mode, ramped in 10 increments. In the displacement control mode, a prescribed displacement of 0.2 in. was applied, also ramped in 10

increments. The point of application is the same as that in the pullout test. Figure D.5 shows the shear test model.

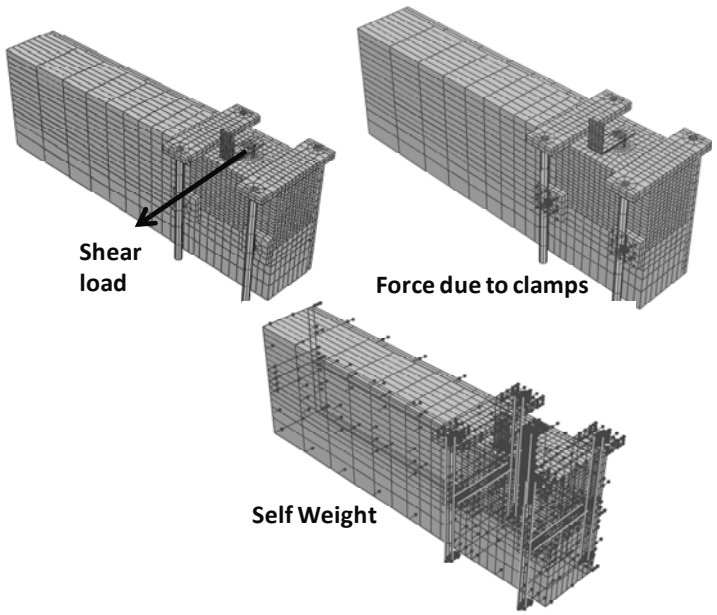

Figure D.5. The shear loading direction.

In the shear loading test, a body force to model the self weight of concrete is applied to the whole beam. Its magnitude is equal to 0.087 lb/in^3. Also, a pressure force of magnitude 1000 psi is applied on the horizontal anchors to model the force due to horizontal clamps. The direction of both the forces is opposite to the direction of the shear force, as shown in Figure D.5.

D.2.4 Boundary Conditions

Three boundary conditions were applied to the model to prevent the concrete beam from moving freely (see Figure D.6).

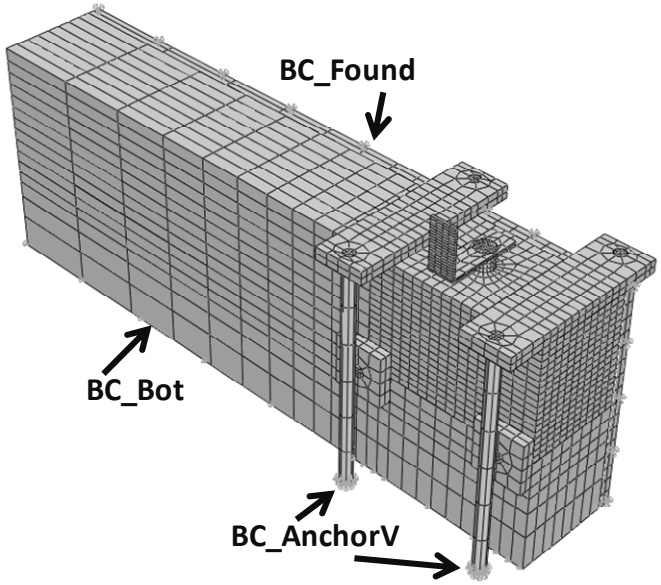

Figure D.6. Boundary conditions.

1. BC_AnchorV was created to keep the vertical fixture clamped to the surface, while the dowel was being pulled out in the pullout test. It restricts the displacement of the edges of the lower surface of the part AnchorV in the x, y, and z-directions.
2. BC_Found was created to keep the horizontal fixture clamped to the surface during the shear test. It restricts the displacement of the edges of the outer surface of the part Foundation in the x, y, and z-directions.
3. BC_Bot was created to keep the concrete beam clamped to the surface while the dowel was being pulled out in the pullout test. It restricts the displacement of the lower surface of the part Bot in the x direction.

D.3 CALIBRATION OF THE BEAM MODEL

D.3.1 Clearance

An important step toward effectively simulating laboratory tests using ABAQUS was to validate certain parameters within the model using laboratory data for similar processes. While doing so, it was discovered that the model showed abnormal behavior for small shear loads. To investigate this effect, an independent beam model was constructed for verification, and the results were compared with laboratory data. One of the most notable ABAQUS parameters affecting model simulations was the contact parameter "Clearance," an internal ABAQUS parameter that defines the maximum distance between the surfaces at which the surfaces are still considered to be in contact. In the case of the beam model developed for this project, the clearance between the concrete beam and the base plate in the shear load testing was found to have significant influence on model accuracy (see Figure D.7). The difficulty in the calibration of the clearance was that the parameter must be small enough to describe the contact realistically, but large enough to keep the model calculations stable. The value of clearance was found to

have a great effect on the shear stiffness results, and thus it should be controlled carefully. Note in Figure D.7 that the results for the clearances at very small values (0.0001 and 0.00001) are numerically coincidental.

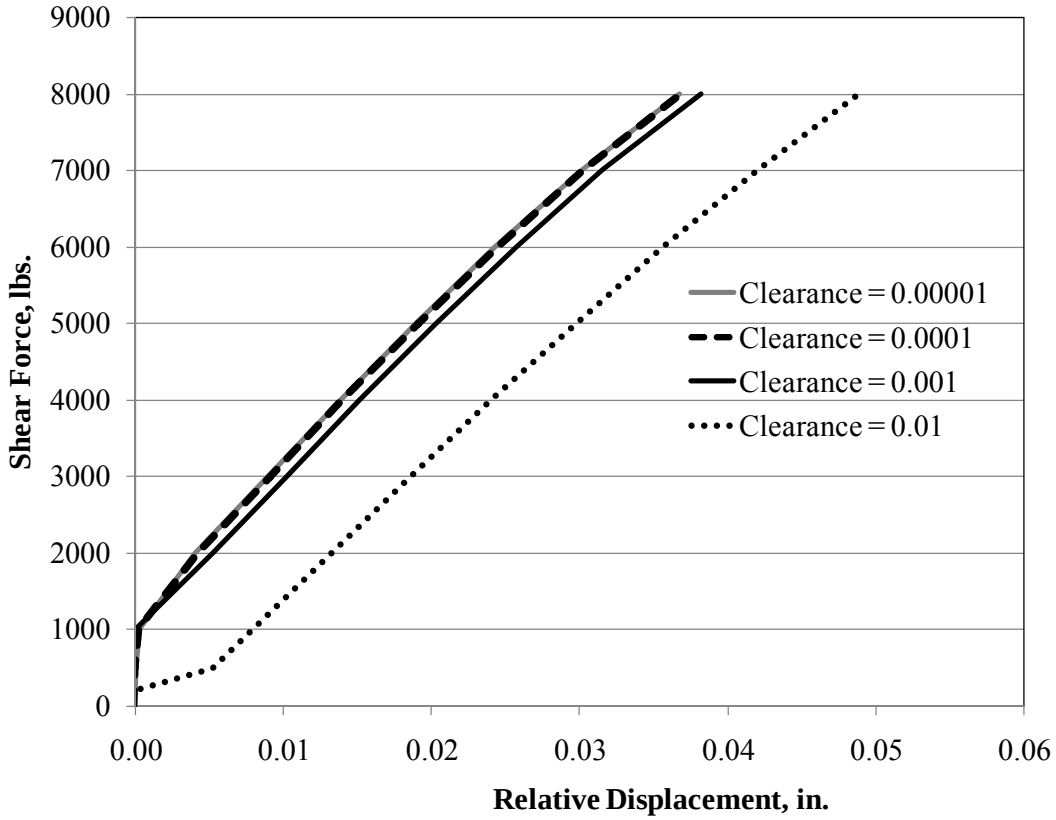

Figure D.7. Effect of clearence input on shear test modeling.

When comparing the laboratory data to the ABAQUS model results, a clearance of 0.01 was chosen as the most accurate representation of the test. Once the clearance issue was resolved, the model satisfactorily replicated the conditions of the laboratory testing. Figure D.8 shows that the shear stiffness between the model and laboratory data is very similar for the perfectly aligned case.

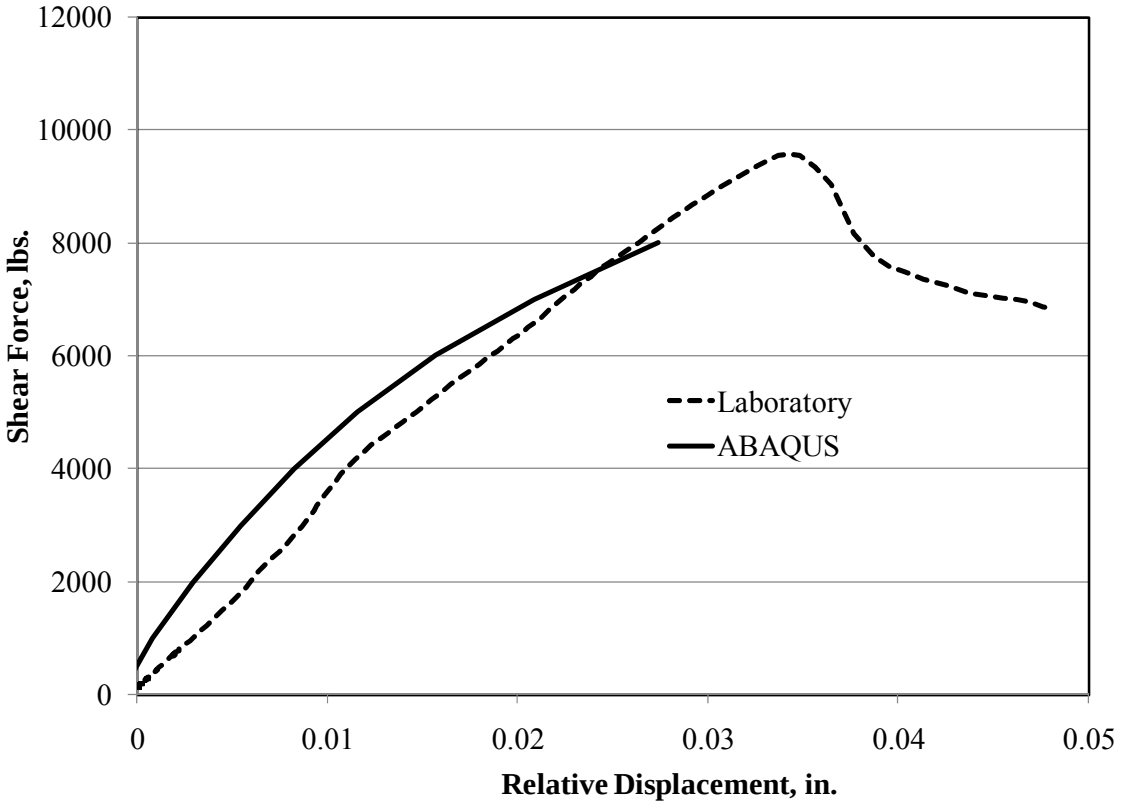

Figure D.8. Comparison of laboratory and model shear pull results for a perfectly aligned dowel.

The model was then altered to be able to account for different types and levels of misalignments. This included reduced embedment length. The shear pull results of the model were similar to the shear pull results in the lab for all of the embedment length cases. Figure D.9 illustrates this agreement for the most extreme case of reduced embedment length (2 in). It can be seen the shear stiffness for the model and laboratory tests is fairly similar.

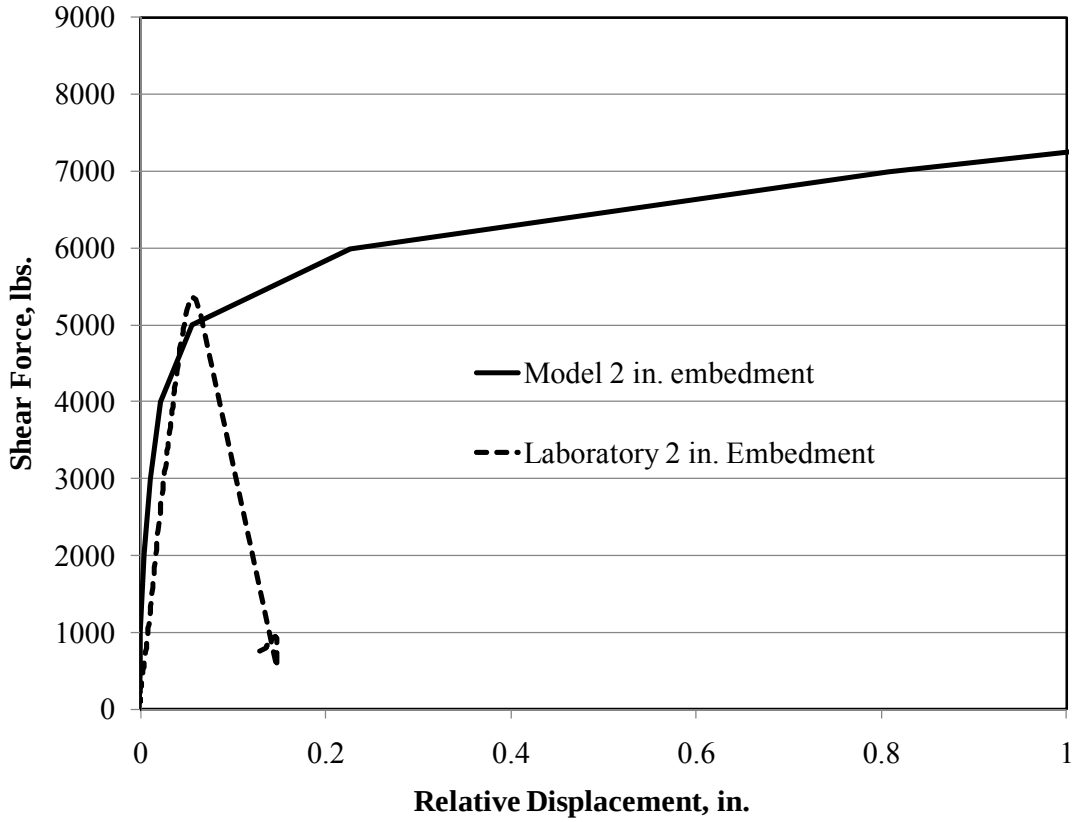

Figure D.9. Model versus laboratory shear pull data for extreme misalignment (2 in).

Therefore, the parameter selected after the calibration of the beam model is clearance between the concrete beam and the base plate needed for shear test fixture. The value for the clearance was selected to be 0.01.

D.4 MODELING MISALIGNMENT FOR THE BEAM MODEL

The various misalignments considered are embedment length (reduced length of the dowel), tilt (vertical or horizontal tilting of the dowel), and translation (reduced or increased concrete cover).

D.4.1 Embedment

For the beam model, embedment length misalignment was modeled by partitioning the dowel into nine pieces of 1 in. each and a single piece of 1.5 in. that remains exposed out of the beam and is fixed to the angle. Dividing the dowel in this fashion allowed the allocation of different material properties to each 1-in. segment. Therefore, for a reduced embedment of say 6 in., the lower 3 in. of the dowel were assigned the material property "Steel2," which has a very low modulus of elasticity. This made it extremely soft compared to the rest of the dowel. Figure D.10 shows the division of the dowel embedded inside the concrete beam.

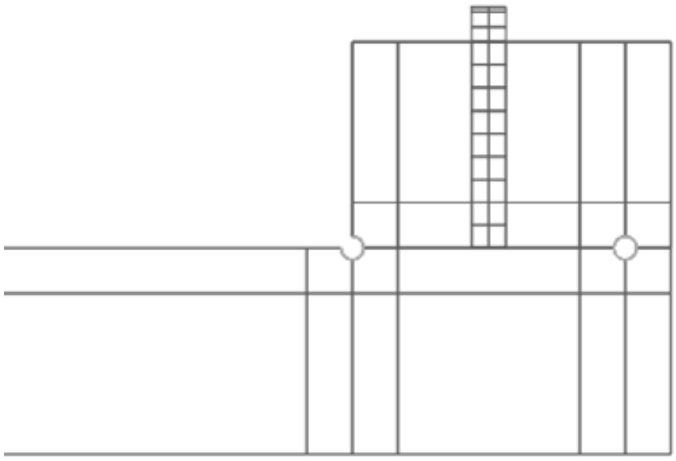

Figure D.10. Top down view of the embedded dowel.

D.4.2 Tilt/Translation

For the vertically/horizontally tilted and translated dowel cases, the model was recreated from the same basic aligned dowel model. This was done by changing the required parameters (coordinates of the reference points of the cut extrude on the concrete surrounding the dowel) in the journal file and regenerating the required model. Different combinations also were modeled using the combination of the above approaches. Thus, the same basic model could be used for all the possible misalignment types and levels. Figure D.11 shows the 1 in. per 9 in. vertical tilt, and Figure D.12 shows the 2 in. translated dowel, equivalent to a concrete cover of 1.25 in. for 1.5 in. dowel diameter.

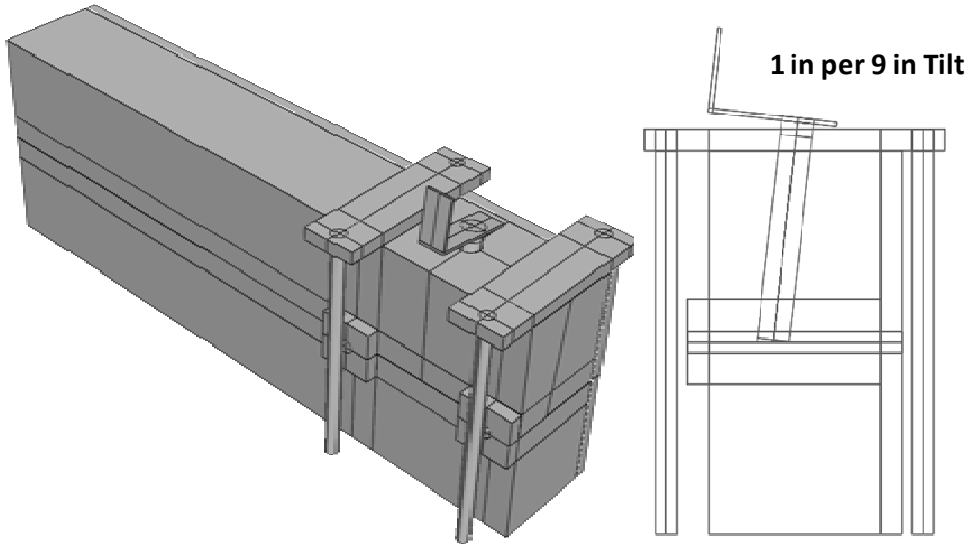

Figure D.11. Beam-dowel assembly with the vertically tilted dowel.

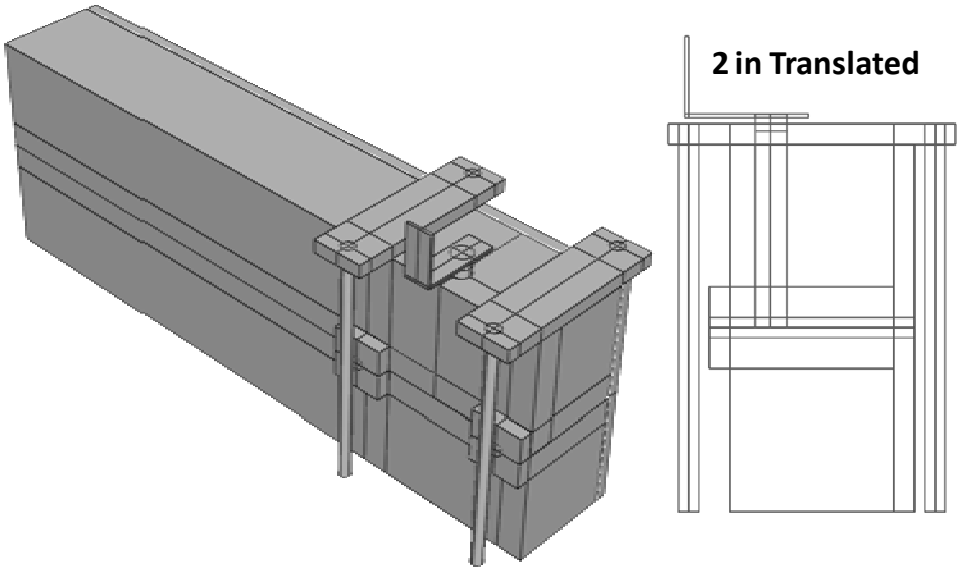

Figure D.12. Beam-dowel assembly with the vertically translated dowel.

D.5 SENSITIVITY ANALYSIS FOR THE BEAM MODEL

A number of cases were simulated to study the effect of various parameters on the beam-dowel model and to calibrate it. The effects of yield stress in tension and compression were calibrated with three different compressive strengths of 4000 psi, 5000 psi, and 6000 psi. For each of the compressive strength, the following relations (Mindess et al., 2003) were used:

$$f_{ce} = 0.7\, f_c' \qquad E = 57000\sqrt{f_c'}$$

where, f_c' = yield strength in compression (psi), f_{ce} = initial yield strength in elastic range (psi), f_t = direct strength in tension (psi), E = modulus of elasticity (psi).

In general, the ratio of the direct tensile strength to compressive strength ranges from about 0.07 to 0.11 (Mindess et al., 2003). The direct tensile strength, f_t was modeled for the following relations:

$$f_t = 0.07\, f_c', \text{ and } f_t = 0.10\, f_c'$$

A stable friction contact between the dowel and the surrounding concrete was ensured using the procedure developed by Khazanovich et al. (2001). According to this procedure, a fictitious temperature is assigned to the dowel to initiate sufficient normal stresses at the dowel-concrete interface. This helps establish the initial contact between the dowel and the concrete surrounding it. Two different fictitious dowel temperatures (15°C and 30°C) were modeled to study the effect of selection of this fictitious temperature on the final pullout and shear test results. Thus a factorial of 12 cases (3 x 2

x 2) was obtained. All the cases run had a dowel diameter of 1.5 in. Table D.1 lists the cases run.

Table D.1. Factorial of strength parameters and fictitious dowel temperature.

Case No.	Concrete Properties (psi)	Direct Tensile Strength f_t (psi)	Fictitious Dowel Temp. (°C)
1	f_c' = 4000 f_{ce} = 2800 E = 3605000	280	15
2			30
3		400	15
4			30
5	f_c' = 5000 f_{ce} = 3500 E = 4030510	350	15
6			30
7		500	15
8			30
9	f_c' = 6000 f_{ce} = 4200 E = 4415200	420	15
10			30
11		600	15
12			30

One aligned and three misalignment cases were considered. The misalignments considered were: 4 in. embedment length, 1 in. per 9 in. of vertical tilt, and 2 in. concrete cover.

Figures D.13 and D.14 illustrate the relative dowel displacement versus load curves for the aligned case in pullout loading. Figure D.13 compares cases 1 and 3, which have the same compressive strength (4000 psi) and fictitious dowel temperature (15°C) but different tensile strengths (280 and 400 psi, respectively). Since the plots superimpose exactly, it can be inferred that the tensile strength is not a sensitive parameter in pullout loading.

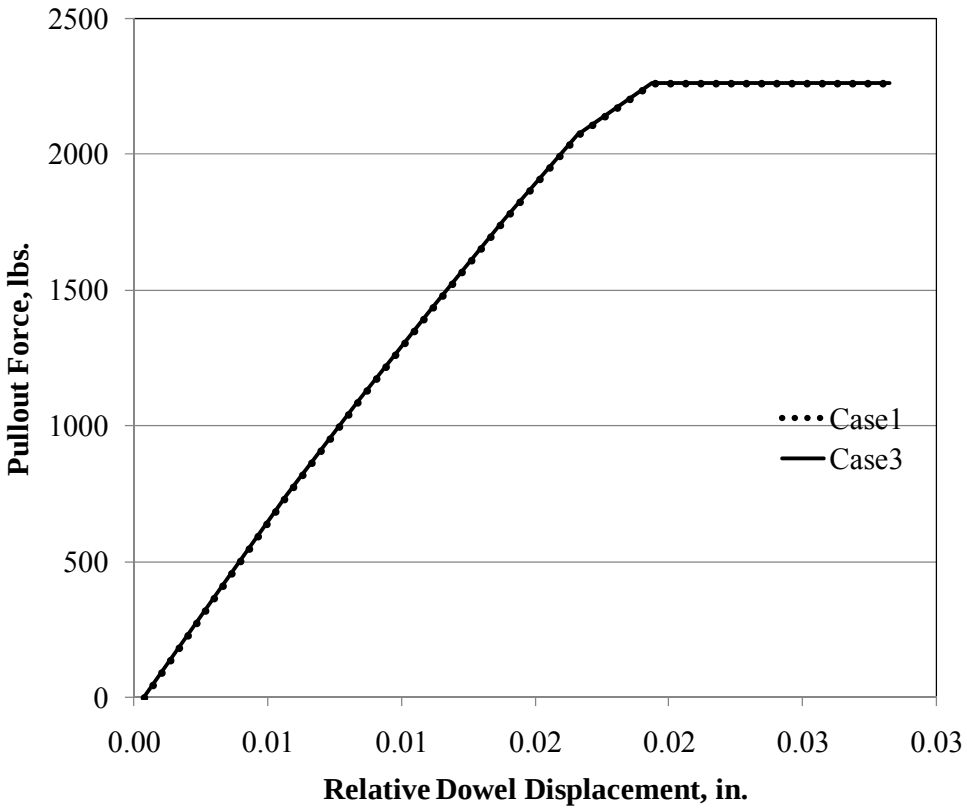

Figure D.13. Aligned case in pullout loading with different tensile strengths.

Figure D.14 compares cases 1, 5, and 9 that have different compressive strengths (4000, 5000, and 6000 psi, respectively) at the same fictitious dowel temperature (15°C). It shows that with the increase in compressive strength, the maximum load taken by the beam increases.

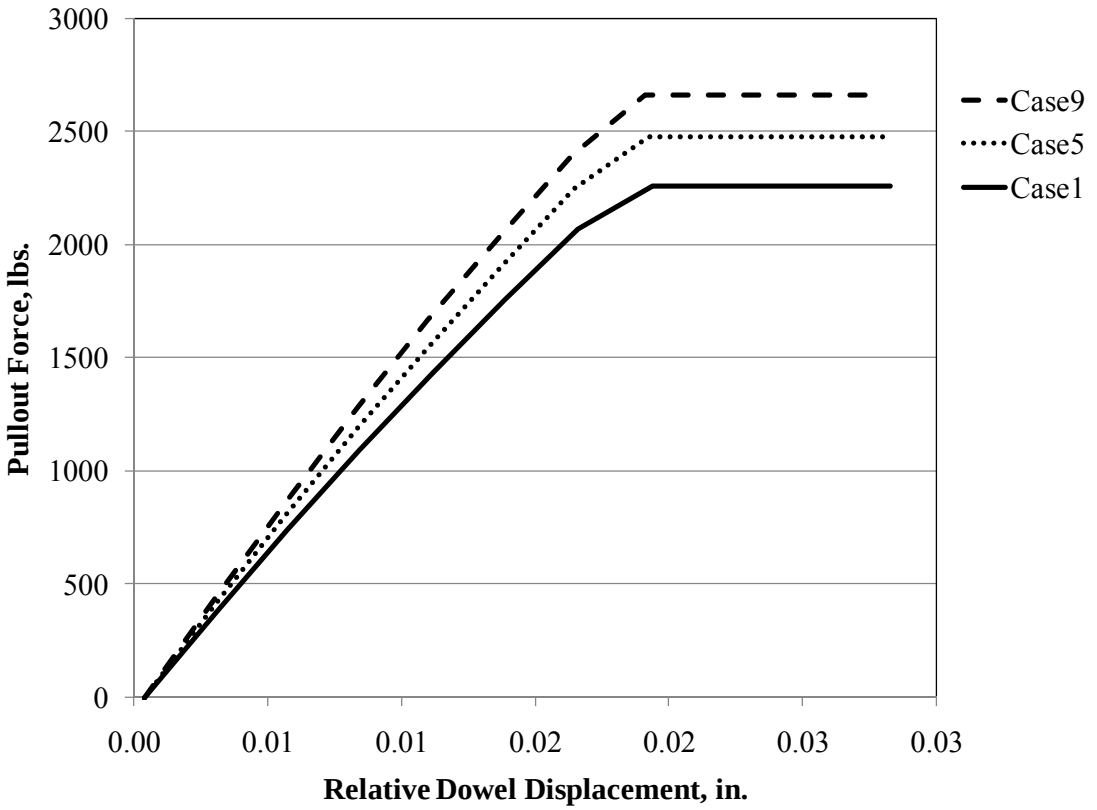

Figure D.14. Aligned case in pullout loading with different compressive strengths.

Figure D.15 shows the relative dowel displacement versus load curves for the aligned case in shear loading. It compares cases 3 and 5 at the same fictitious dowel temperature (15°C). Case 3 has a compressive strength of 4000 psi, while case 5 has a compressive strength of 5000 psi. However, it should be noted that case 3 has a higher tensile strength (400 psi) than case 5 (350 psi). As seen in Figure D.15, the maximum load taken by case 5 is lower than that for case 3. Thus, the shear load test is sensitive to the direct tensile strength of the concrete.

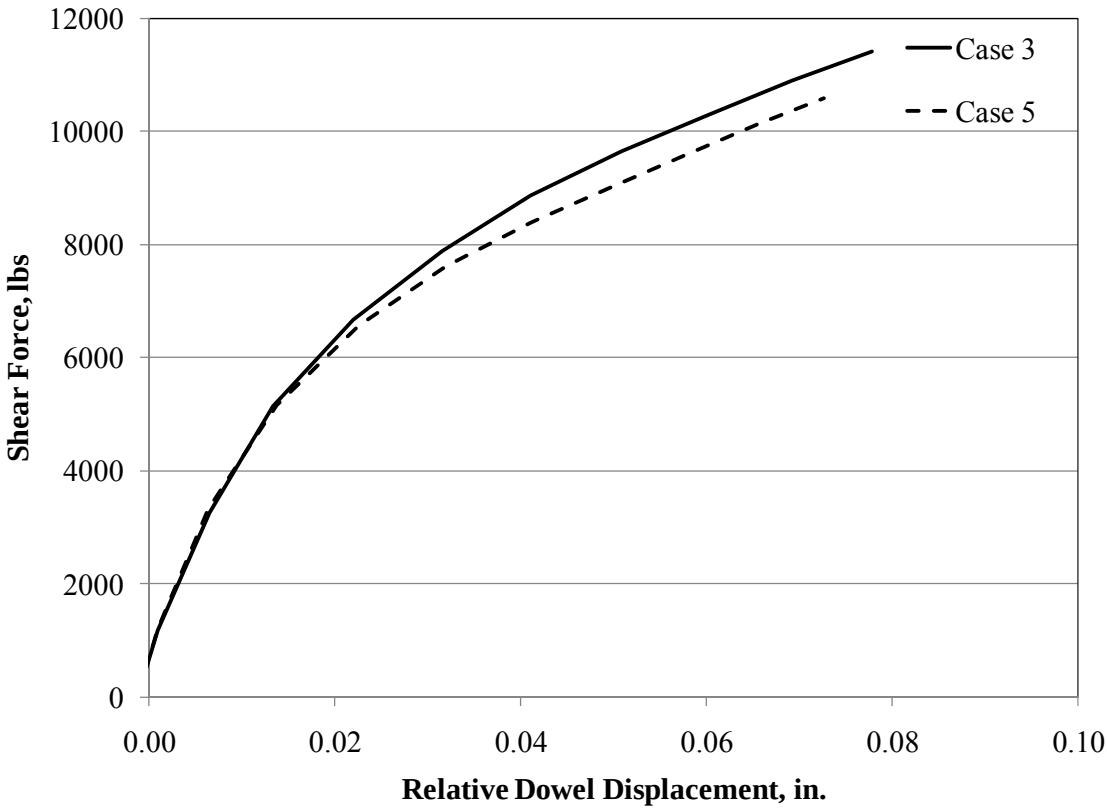

Figure D.15. Aligned case in shear loading.

Figures D.16 and D.17 show the relative dowel displacement versus load curves for a 4 in. embedment case in pullout loading and a 2 in. concrete cover case in shear loading, respectively. Figure D.16 compares cases 1 and 2 in. pullout loading. These cases have the same compressive strength (4000 psi) and the same tensile strength (280 psi). Case 1 is subjected to a fictitious dowel temperature of 15°C, while case 2 has a fictitious dowel temperature of 30°C. For the pullout testing, it can be seen in Figure D.16 that the fictitious temperature to which the dowel is subjected initially changes the maximum load taken by the beam-dowel assembly.

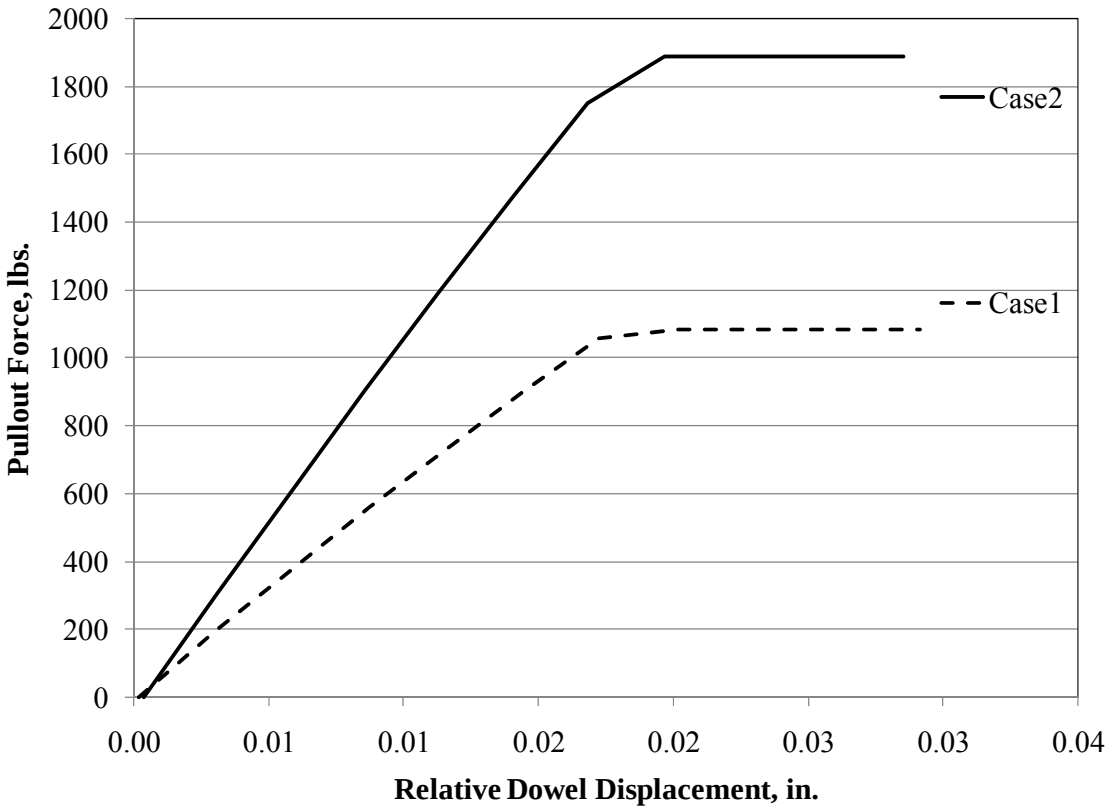

Figure D.16. Four-in. embedment in pullout for different fictitious dowel temperatures.

Figure D.17 compares cases 9 and 10 that have the same compressive strength (6000 psi) and tensile strength (420 psi). Case 9 has a fictitious dowel temperature of 15°C, whereas case 10 has a fictitious dowel temperature of 30°C. As both the curves superimpose each other, it can be inferred that the fictitious dowel temperature does not affect the shear loading.

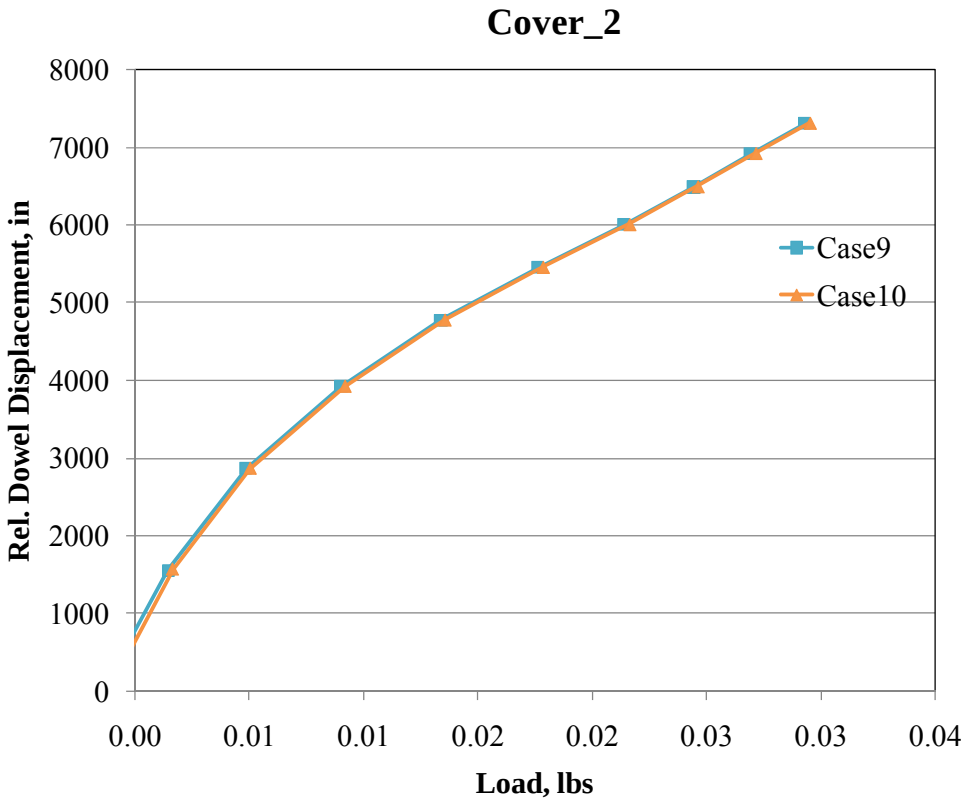

Figure D.17. 2 in. concrete cover in shear test for different fictitious dowel temperatures.

The pattern observed in Figures D.13 through D.17 was exactly the same for all the cases of misalignments considered.

D.5.1 Results from Sensitivity Analysis

The results obtained from the pullout and shear load testing for aligned dowels had a specific pattern for the factorial of simulations. This pattern is summarized below. This pattern was exactly the same for results of the factorial for the misaligned dowel cases, irrespective of the type or level of misalignment. This implies that the misalignment level and types are not sensitive to the physical properties of the materials used in the beam model.

It was observed that:

- Tensile strength does not affect the ultimate load or the stiffness during pullout loading simulations. Thus, the tensile strength is not a sensitive parameter for the pullout test.
- In the simulated pullout test, the maximum load taken by the beam increases with an increase in the compressive strength. Thus, the compressive strength of concrete is a sensitive parameter for the pullout test.

- For the shear loading test simulations, the maximum load taken by the beam increases with an increase in the direct tensile strength. Thus, the shear load test is sensitive to the direct tensile strength of the concrete.
- For the pullout test simulations, an increase in the fictitious temperature causes the maximum load taken by the beam to increases. Thus, choosing a proper fictitious temperature is critical to the modeling of the pullout test.
- The fictitious temperature has no observable effect on the results for the simulated shear test.

It bears repeating that these parameters exhibit similar results for the misaligned dowels, where the misalignment of the dowel was expressed in terms of embedment length, vertical tilt, or modified concrete cover.

D.6 RESULTS FROM FINITE ELEMENT ANALYSIS FOR THE BEAM MODEL

This section presents the results from the FEM analysis of the beam. As detailed in earlier sections, the beam model successfully matched the results from the laboratory tests. Thus, with a validated model, a number of simulations beyond the laboratory tests were attempted for a variety of dowel misalignment magnitudes and types.

A comparison of the measured pullout force in the laboratory and predicted pullout force using ABAQUS is presented in Figure D.18. One can observe a few differences in the laboratory data and the simulated data from the FE beam model:

- The laboratory measured pullout force exhibited unstable behavior after a certain level of dowel displacement. This behavior can be attributed to dynamic slip. Modeling this phenomenon using ABAQUS would dramatically increase the complexity of the finite element model without providing a corresponding benefit to the project.
- The measured pullout forces from the laboratory varied significantly. The dowel/concrete friction model parameters were selected based on past experience (Khazanovich et al., 2001). Figure D.18 demonstrates that the predicted pullout force is within the limits of the measured pullouts forces.

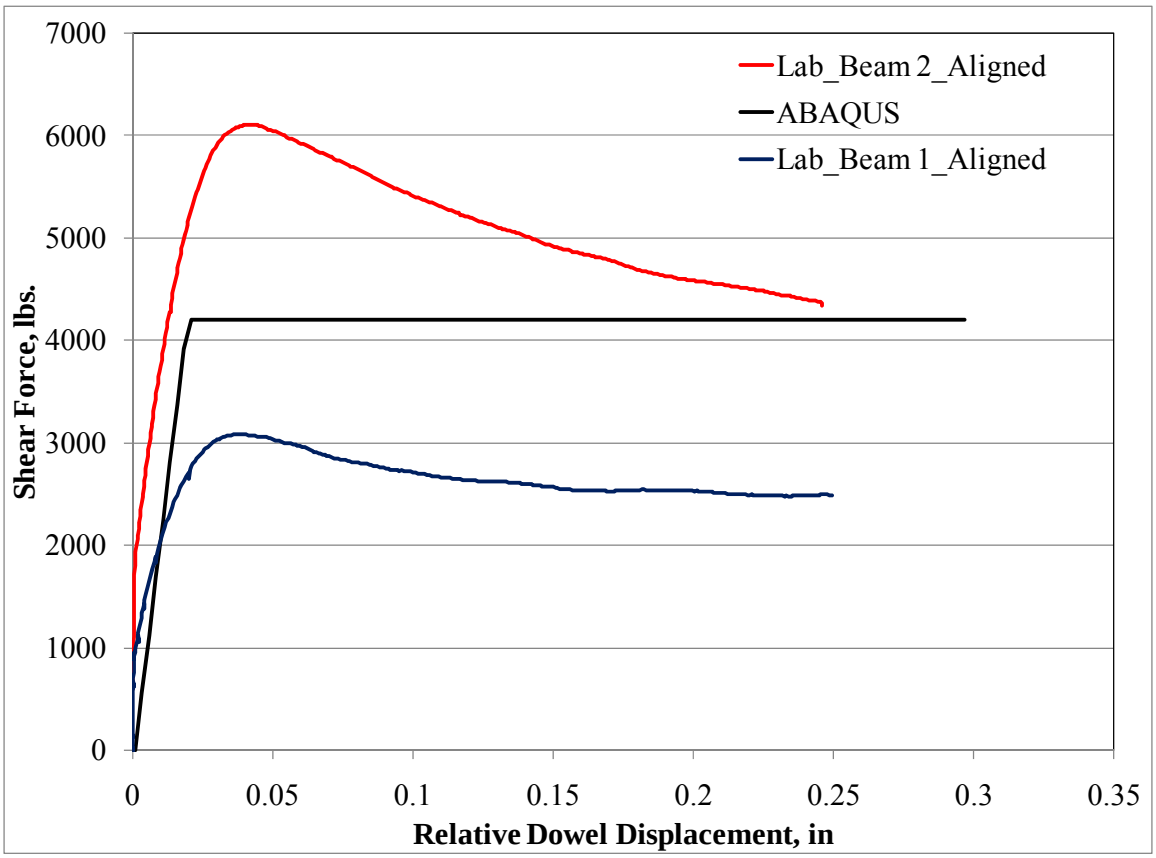

Figure D.18 Comparison of laboratory and model pullout test results for aligned dowel.

Figure D.19 displays the relative displacements versus shear force for an aligned dowel tested in shear in the laboratory and simulated using ABAQUS. The Figure shows that the model and laboratory data are similar for the aligned dowel case. Figures 2.23 and 2.24 in the report showed that simulated model data and laboratory data correspond well in describing the shear force versus dowel displacement for low embedment length.

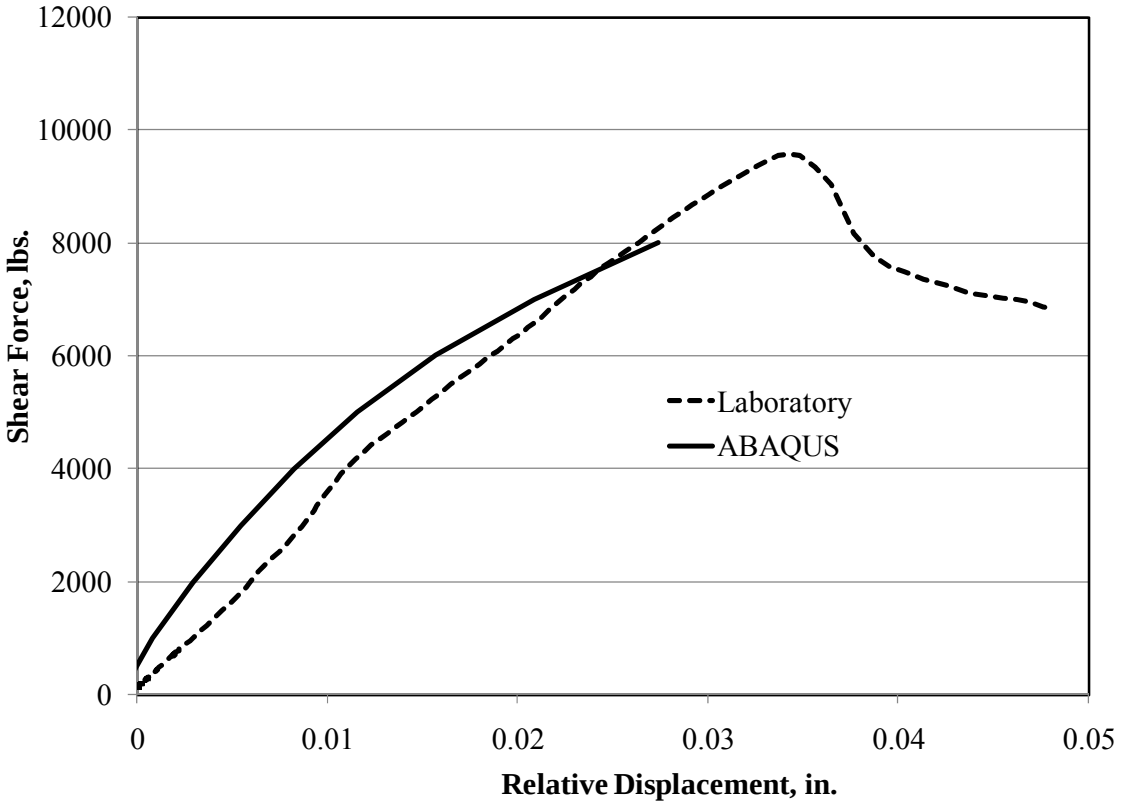

Figure D.19 Comparison of laboratory and model shear pull results for aligned dowel.

Section 3.3.1 of the report illustrated the results of the FE analysis of the beam model with respect to different types and values of misalignment. Figures 3.26, 3.27, 3.28, and 3.29 showed the shear capacity levels for different embedment lengths, concrete covers, dowel diameters, and vertical tilts respectively. It was observed that a reduction in embedment length and concrete cover reduces the dowel shear capacity. Reducing the dowel diameter also reduced the dowel shear capacity, as expected. For the vertical tilt cases, no significant effect of dowel rotation was seen on the dowel shear capacity until the rotation becomes unrealistically large. However, the beam model does not take into account the effects of interaction of multiple dowels present in a slab joint.

The combined effect of the various misalignments also was studied. Figure D.20 shows the relative dowel displacement versus load in shear pull test for 3, 6, and 9-in. embedment lengths with a vertical tilt of 1 in. per 9 in. of the dowel length. The dowel shear capacity reduced with the decrease in embedment length.

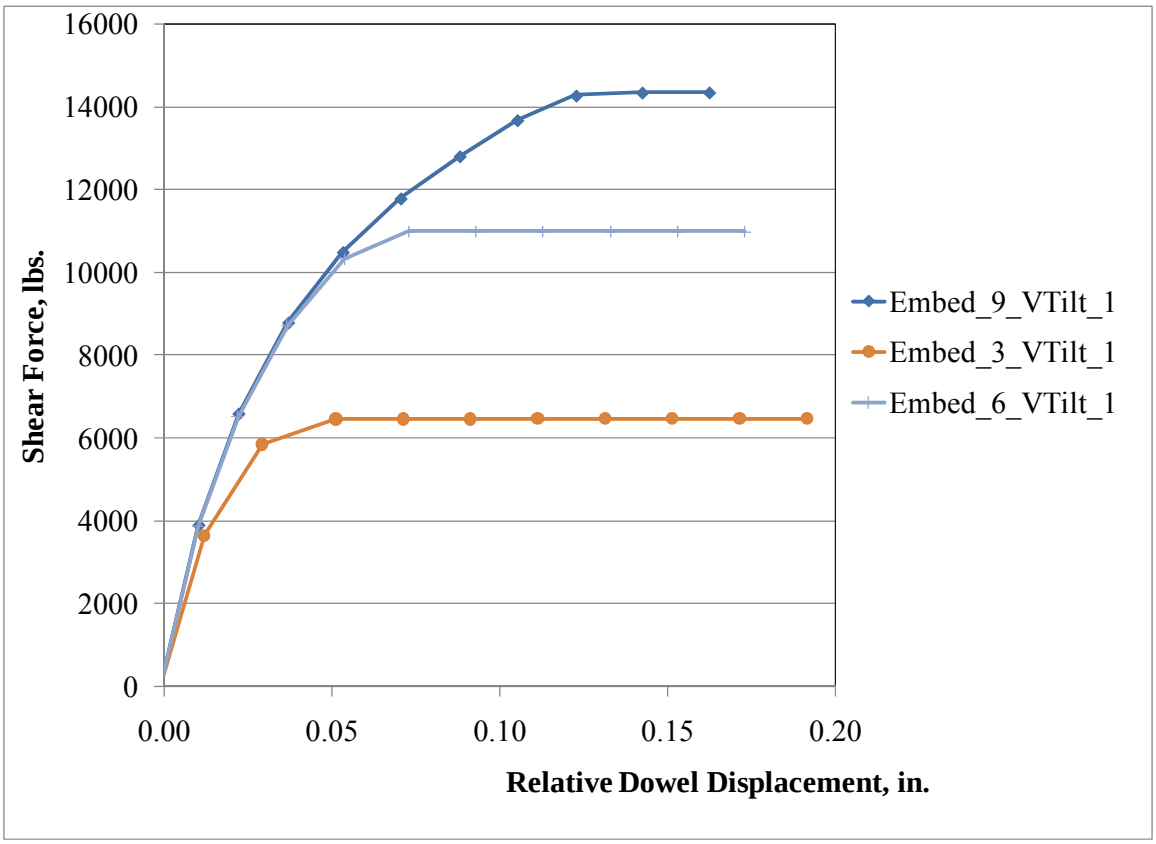

Figure D.20. Shear capacity for the different levels of embedment lengths with 1 in. per 9 in. vertical tilt.

Figure D.21 shows the relative dowel displacement versus shear load in a shear pull test for 3, 6, and 9-in. embedment lengths with a very low concrete cover of 1.25 in.. These cases failed even before the relative dowel displacement reached 0.05 in. (the value that was selected to represent the effective dowel shear capacity for this study). This was an extreme case of misalignment with very low embedment lengths (3 and 4 in) and a very low concrete cover (1.25 in).

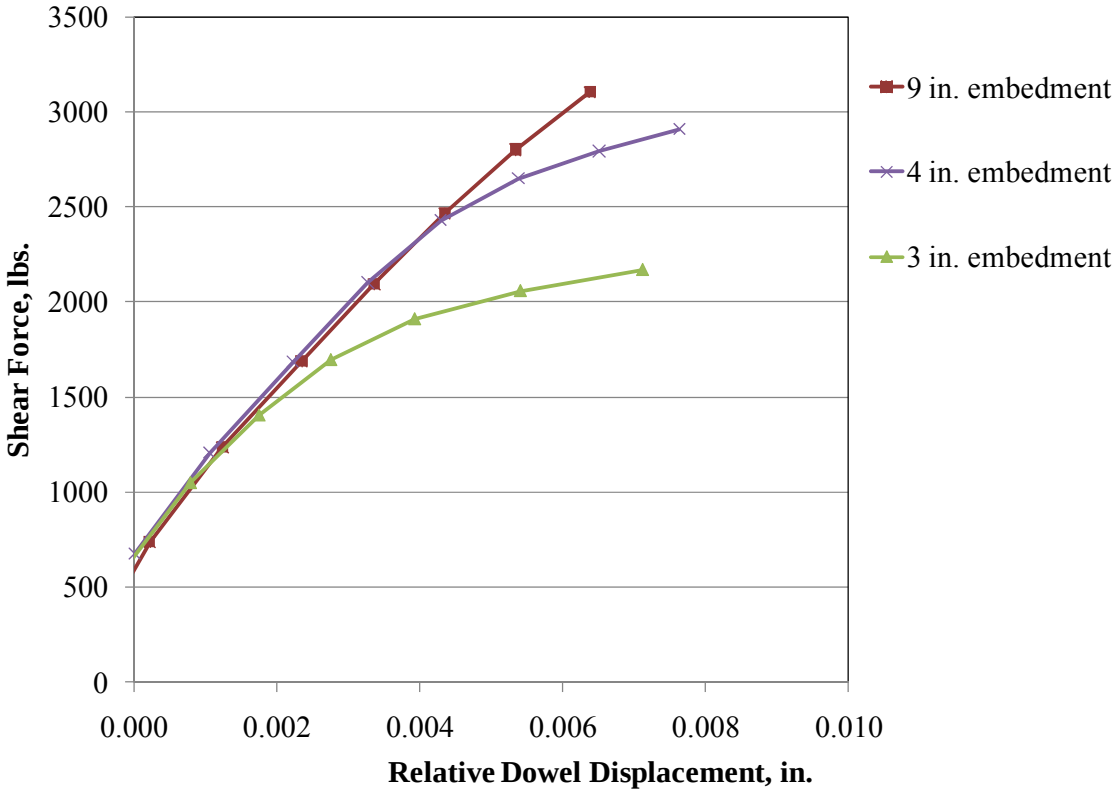

Figure D.21. Different levels of embedment lengths with 1.25 in. concrete cover.

Figure D.22 shows the results from the shear pull test for dowel diameters ranging from 1.0 in. to 1.5 in. for an embedment length of 5 in.. The dowel shear capacity decreased with the reduction in dowel diameter.

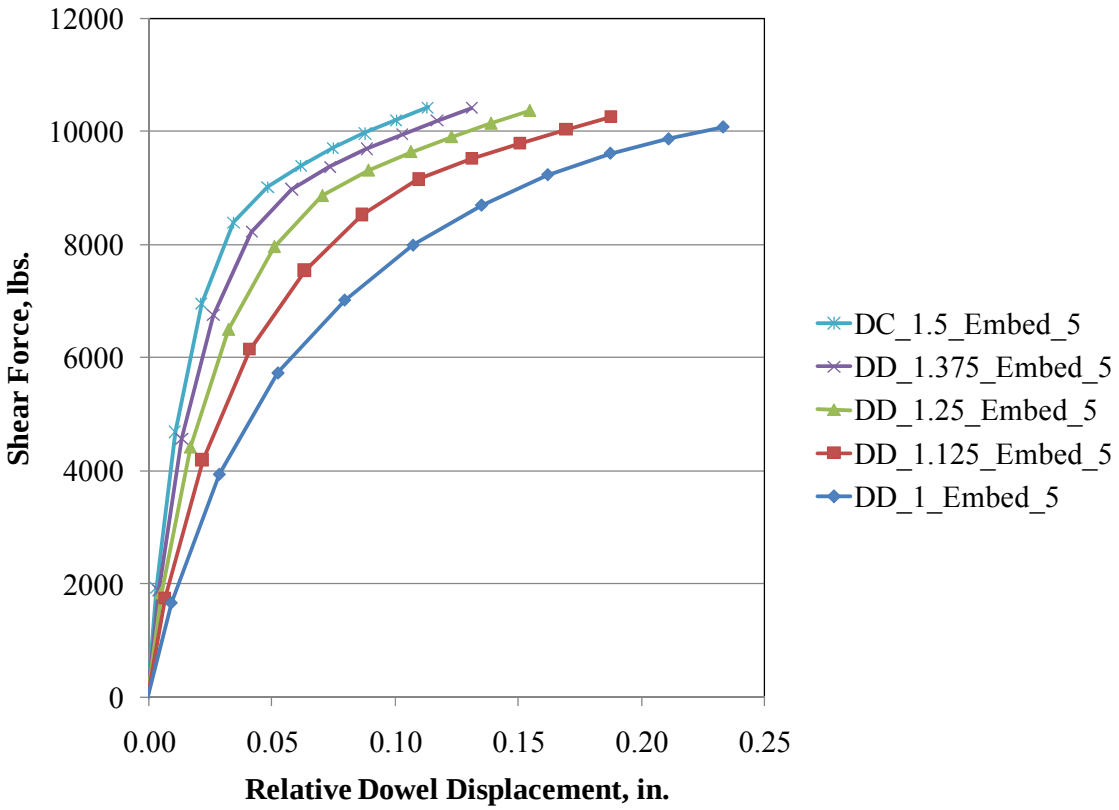

Figure D.22. Shear capacity for the different dowel diameters with 5 in. of dowel embedment length.

Figure D.23 shows the shear pull test results for concrete cover cases ranging from 1.375 in. to 7.375 in. for a dowel diameter of 1.25 in.. The dowel shear capacity reduced with the decrease in concrete cover, a trend similar to as seen for the 1.5 in. dowel diameter case with varying concrete covers.

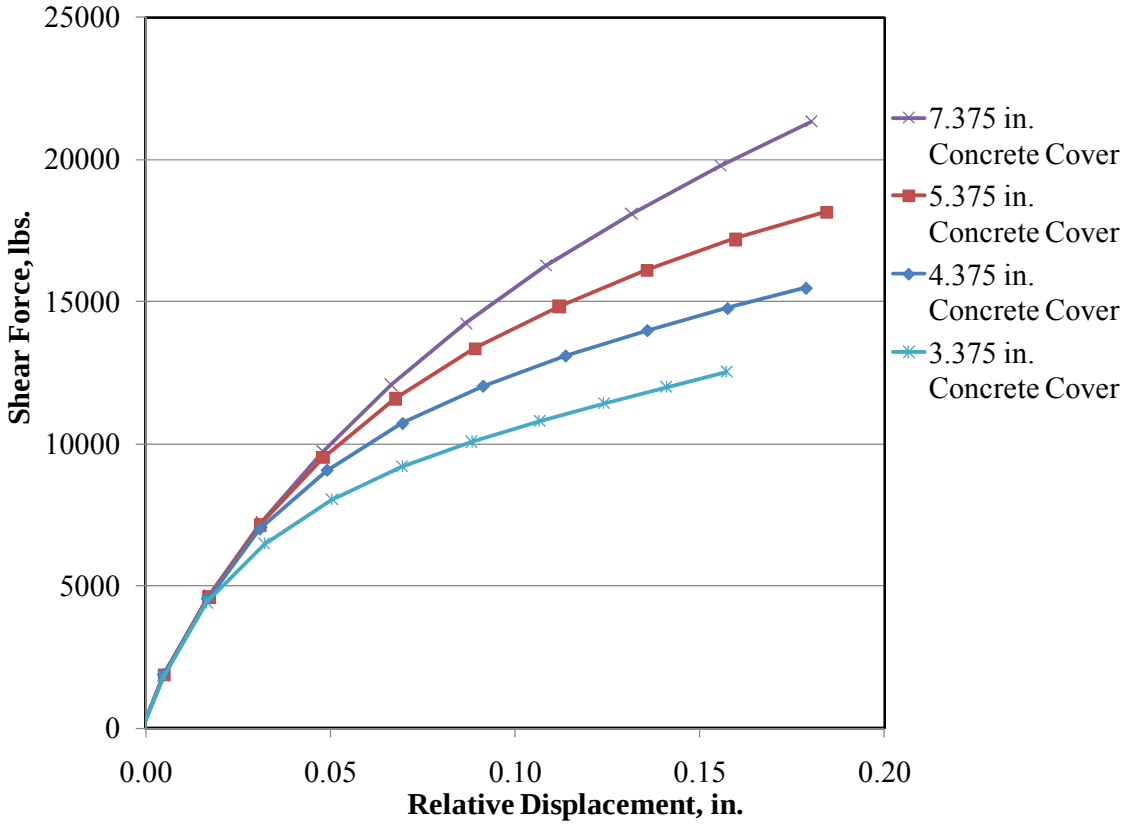

Figure D.23. Shear capacity for the different concrete cover for 1.25 in. dowel diameter.

D.7 SLAB MODEL

The beam model was expanded to a slab model to investigate the effect of rotations, in the form of horizontal skew and vertical tilt, due to multiple dowels in the joint. The slab model was designed to simulate temperature expansion and contraction, as well as wheel loading at the joint. The total number of elements used was 30,464 of type C3D8R, which is an eight-node, reduced-integration 3D linear brick element. Multiple parts were used to assemble the model. The model consists of two slabs connected by the dowels at the joint. The dimensions of the slabs are shown in Figure D.24.

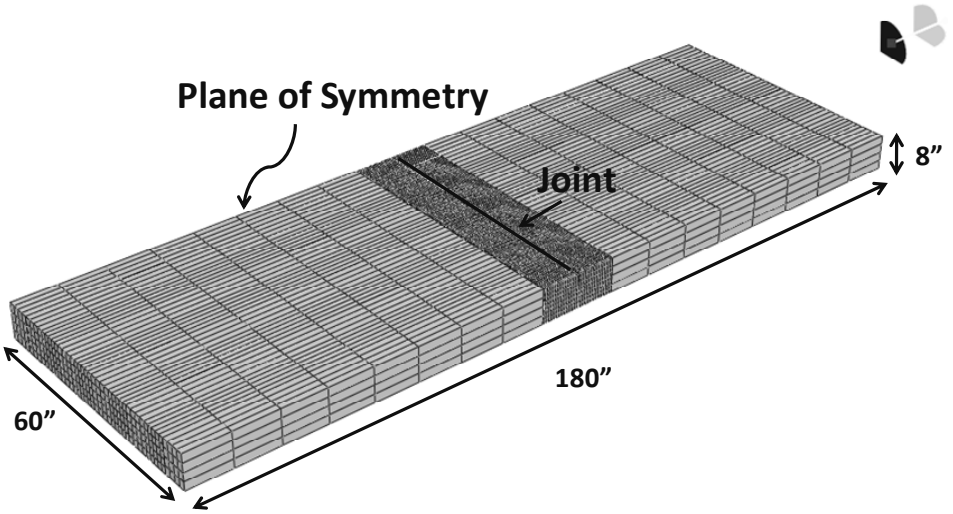

Figure D.24. Slab model.

D.7.1 Parts and Material Properties

The slab model consisted of five 3D deformable parts (see Figure D.25 and the descriptions that follow). The bottom part was a regular concrete block with no holes. The top part had a cut extrude for the dowel to go through it. Two concrete blocks, side bottom and side top, similar to the bottom and top parts respectively, but half in width and without a cut extrude were added to the model on either side. The dowel was virtually partitioned into 18 parts of 1 in. each to model the embedment length misalignment.

Unlike the beam model, it did not have any horizontal or vertical fixtures, but the use of symmetrical boundary conditions along one of the longitudinal planes mapped the same effect. To limit the effect of the reduction in slab length in the longitudinal direction, the ends of the slab along the outside longitudinal edges were constrained by springs. The slab was supported on an elastic foundation, which was modeled using distributed springs.

The slab consisted of five parts: bottom, top, dowel, side bottom and side top, as shown in Figure D.25. The bottom part was a regular concrete block with no holes. The top part had a cut extrude for the dowel to go through it. Two concrete blocks, side bottom and side top, similar to the bottom and top parts respectively, but half in width and without a cut extrude were added to the model on either side. The dowel was virtually partitioned into 18 parts of 1 in. each to model the embedment length misalignment. The model consists of five 3D deformable parts, namely:

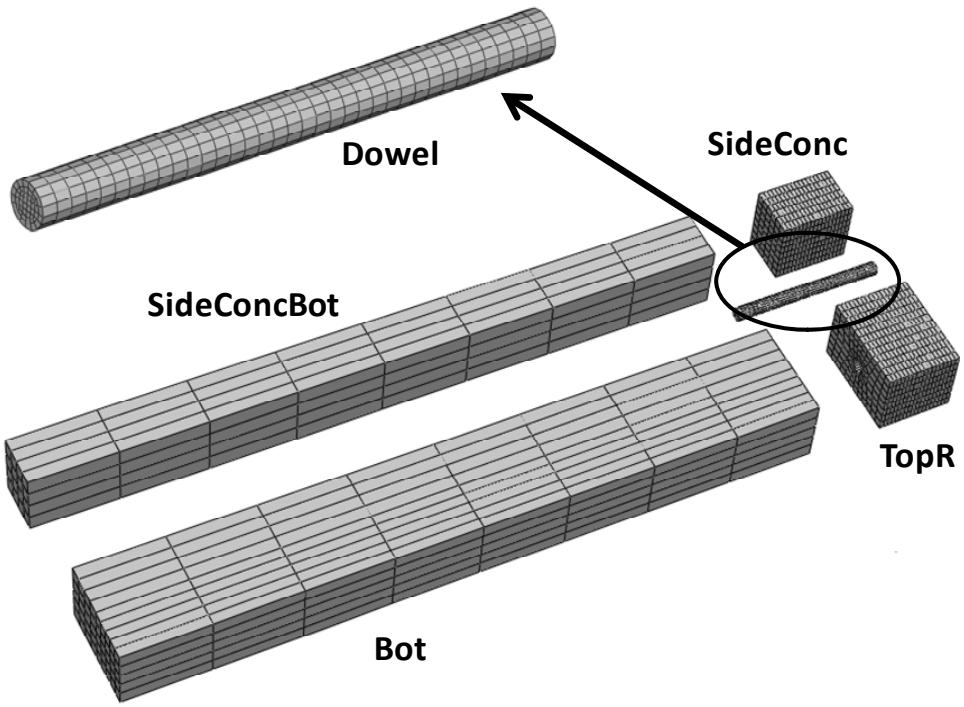

Figure D.25. Parts of the slab model.

1. Bot (bottom part) – The solid extrude has a dimension of 81 x 12 x 8 in. Eight instances of this part have been used in the assembly. The mesh has 360 elements. The material property assigned to this part is "Concrete2," the same as in the Bot part of the beam model.

2. TopR (top part) – This part contains the dowel. The solid extrude has a dimension of 9 x 12 x 8 in. The central cut extrude has a radius of 0.75 in, and it is a blind cut 9 in. deep. It is drawn using two datum points, a datum axis and a datum plane. Eight instances of this part have been used in the assembly. The mesh has 2088 elements. The material property assigned to this part is "Concrete," the same as in the TopR part of the beam model.

3. Dowel – The solid extrude has a depth of 18 in. and radius of 0.75 in.. Four instances of this part have been used in the assembly. The mesh has 1728 elements. The material property assigned is "Dowel," the same as in the Dowel part of the beam model.

4. SideConc (side top part) – This part is attached next to the part "TopR," along both longitudinal edges of the slab. The solid extrude has a dimension of 9 x 6 x 8 in. Four instances of this part have been used in the assembly. The mesh has 864 elements. The material property assigned to this part is "Concrete."

5. SideConcBot (side bottom part) – This part is attached next to the part "Bot," along both longitudinal edges of the slab. The solid extrude has a dimension of 81 x 6 x 8

in. Four instances of this part have been used in the assembly. The mesh has 128 elements. The material property assigned to this part is "Concrete2."

D.7.2 Contact Interactions

The slab model has only one contact interaction, *dowel-concrete interaction*, between the dowel and the concrete surrounding it. The interaction is modeled in the same way as in the beam model.

D.7.3 Procedure for Modeling of Dowel Misalignment in the Slab Model

The method to rotate the dowel in the slab in horizontal or vertical tilt is detailed as follows; all possible combinations can be generated by following the procedure. Each part containing the dowel is modeled independently as TopR, TopR2, TopR3, and TopR4. These are similar to the part "TopR" in the beam model. The purpose of doing so is to create independent reference planes for each concrete cut extrude containing the dowel to model different magnitudes and directions of tilt at the same time. The coordinates of the reference points on the reference plane can be changed according to the required tilt. Thus, by rotating any individual reference plane, we can change the direction of the individual cut extrude. Since the dowel is coaxial with the cut extrude in the concrete, it tilts as required.

D.7.4 Boundary Conditions

The slab rests on an elastic Winkler foundation. A symmetry boundary condition was applied along one of the longitudinal edge of the slab, making the effective slab width 120 in. This also helped to cut the run time of the slab model in half without any loss in accuracy.

D.7.5 Loading

To initiate the dowel-concrete contact, the same procedure was used as in the beam model. After that, prescribed longitudinal displacements were applied at opposite transverse edges of the modeled slab to simulate temperature contraction of the concrete slabs (see Figure D.26).

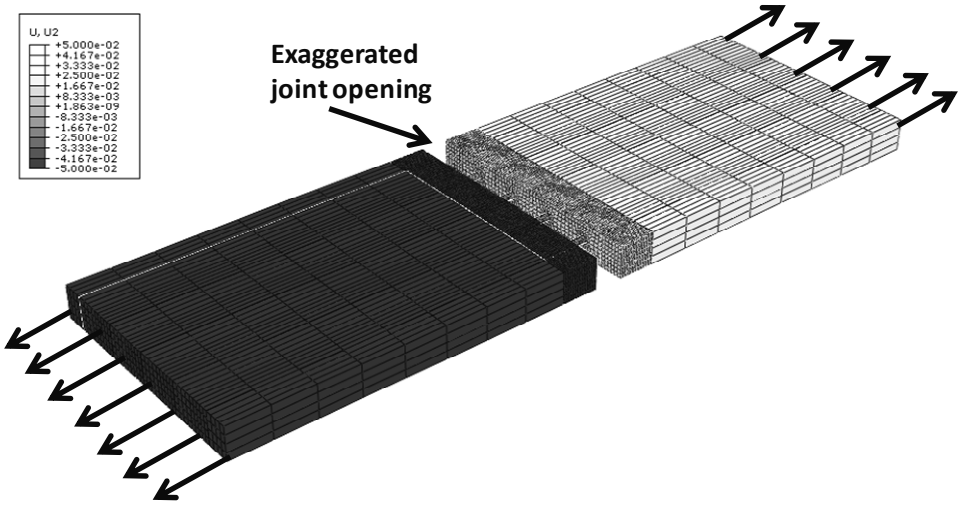

Figure D.26. Pullout mode of the slab showing exaggerated joint opening.

The resulting joint opening induces damage in the concrete surrounding the misaligned dowels. Figure D.27 compares the stresses in the concrete surrounding the dowels in the joints with aligned and the vertically tilted in opposite directions dowels. One can observe that at the end of the joint opening step, the concrete stresses around misaligned dowels are higher than the concrete stresses around the aligned dowels.

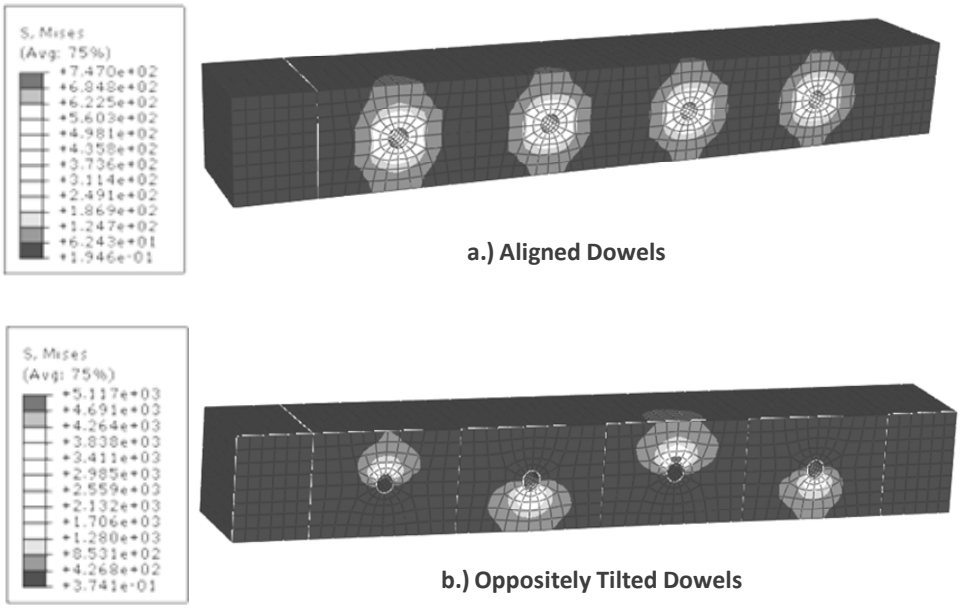

Figure D.27. Mises stresses in the concrete around the dowels. a) joint with aligned dowels b) joint with oppositely tilted dowels.

After the joint opening was simulated, the prescribed displacements were deactivated, and the wheel load was then applied at the corner of the slab. This caused displacements of the system, as shown in Figure D.28. The ratio of displacements of the loaded and unloaded slabs due to the wheel loading was used to measure the load transfer efficiency for different levels of dowel rotation.

$$LTE = \frac{d_u}{d_l} * 100\% \quad \text{(D.1)}$$

where

d_l is the deflection at the joint of the loaded slab (6 inches away from the corner);
d_u is the corresponding deflection at the joint of the unloaded slab; and
LTE is the joint load transfer efficiency.

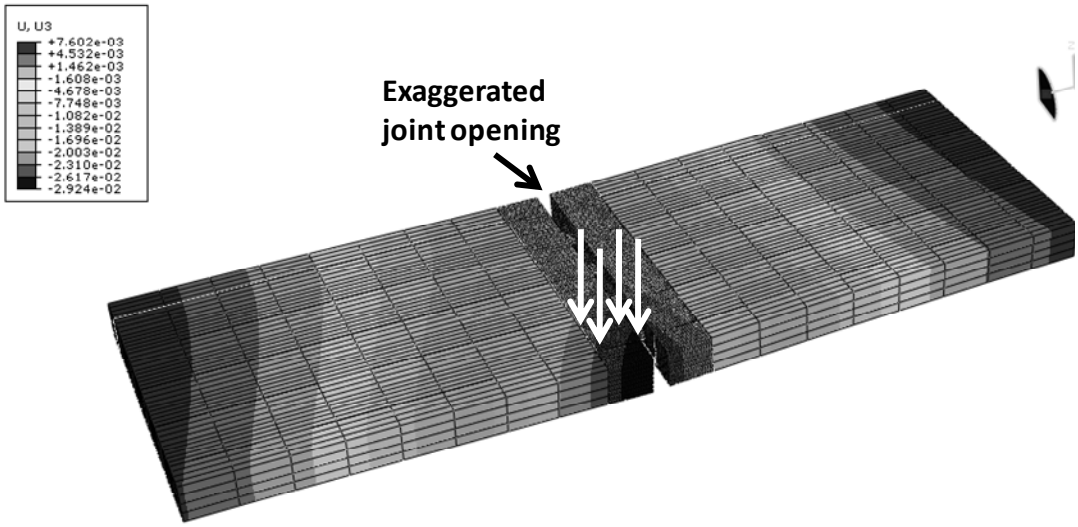

Figure D.28. Wheel loading mode of the slab showing exaggerated joint opening.

D.7.6 ISLAB2000 Model

The ABAQUS slab model has a smaller slab size, a half-axle loading, and is simulated by a single wheel 9-kip load. To evaluate the robustness of the model, the outcomes were compared with the numerical results from the finite element model ISLAB2000. The ISLAB2000 model had four slabs (two in longitudinal and two in transverse directions) loaded by an 18-kip single axle load with dual tires. Each slab was 15 ft long and 12 ft wide. The transverse joint was modeled as a doweled joint with dowels placed every 12 in. The longitudinal joint was modeled as an aggregate interlock joint. The load was placed at the transverse joint with the outer wheel placed at the slab corner. Figure D.29 presents the ISLAB2000 finite element mesh along with the load and dowel locations.

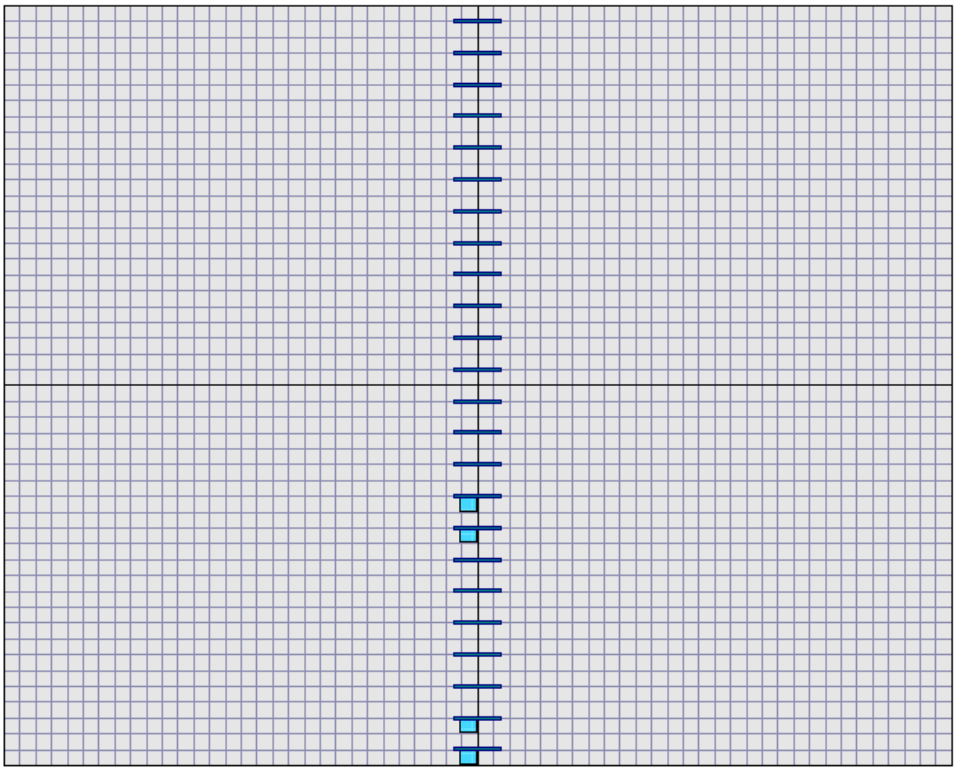

Figure D.29. ISLAB2000 finite element mesh.

A factorial of ISLAB2000 runs was performed for this model with the dowel diameters varied from 1 to 1.5 in. The corner deflections of the unloaded slab deflections were obtained from each simulation, and the corresponding LTEs were computed using equation D.1. These LTEs were compared with the LTEs obtained for the same dowel diameters from the ABAQUS slab model. Figure D.30 presents a comparison of the results. One can observe that the models' predictions are very close. This comparison shows that the ABAQUS slab model is not limited by a smaller slab size and corresponding number of dowels approximation.

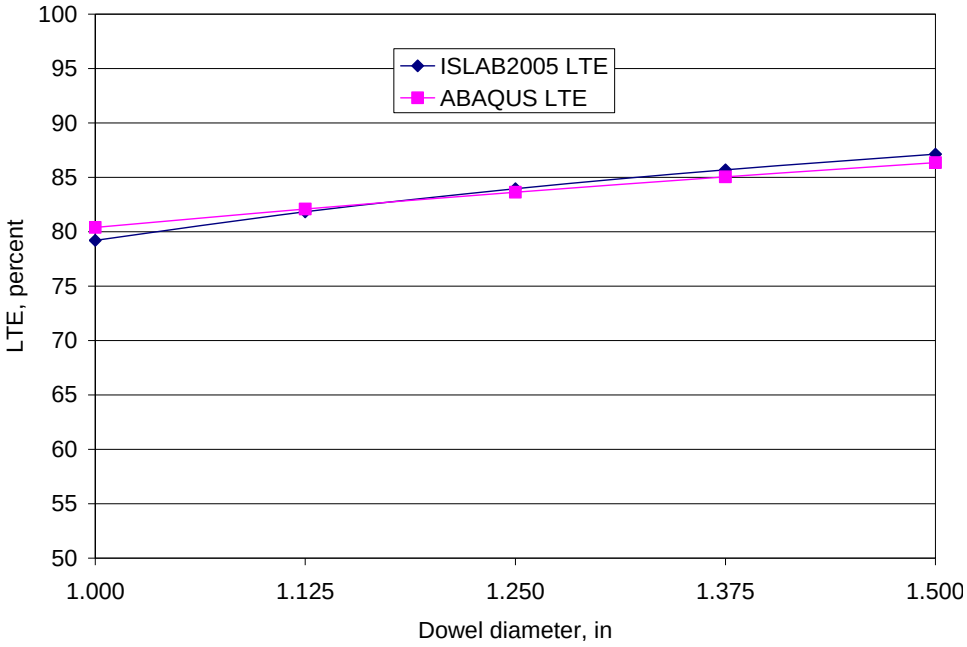

Figure D.30. Comparison of LTEs from ABAQUS and ISLAB2000 models.

D.7.7 Effect of the Mesh Size on Accuracy and Computation Time

Four dowels were used in the slab model along the joint. The number of dowels to be put in the model was selected by taking into consideration the running time. Adding more dowels increased the number of elements proportionally and resulted in even greater computational time. Also, two different meshes in the vicinity of each dowel were compared, namely a coarse mesh with 1044 elements in the concrete and a fine mesh with 2088 elements in the concrete. The fine mesh case with four dowels (the total number of elements in the slab model is 30464) required approximately 4 hours of runtime on a University of Minnesota supercomputer with two processors allocated for the job. The runtime on the coarse mesh (the total number of elements in the slab model is 22112) was about 2 hours.

Figure D.31 presents a comparison of the LTE obtained from the slab models using both a fine and coarse mesh for the concrete surrounding the misaligned dowel. For a low level of misalignment, both models yield similar results. However, as the misalignment becomes more severe, the results for the LTE in these two cases become quite different. At the point that the vertical tilt exceeds 1.5 in. per 18 in. in length, the coarse mesh model produces a jump in LTE. This jump is most likely due to an insufficient number of elements in this critical region, which leads to corresponding errors in the LTE as computed by the finite element model. Although the fine mesh model also exhibits this jump, the additional elements in this critical region appear to reduce the magnitude of this jump and produce more accurate results. Therefore, in spite of the required additional computational time for the finer mesh, the higher mesh density allowed for more accurate analysis of the strains, stresses, and deflections at the most relevant points. At the same time, further refinement of the model was concluded to be impractical due to

computational limitations. The fine mesh case was selected for this slab analysis as a compromise between accurate results and efficient run time.

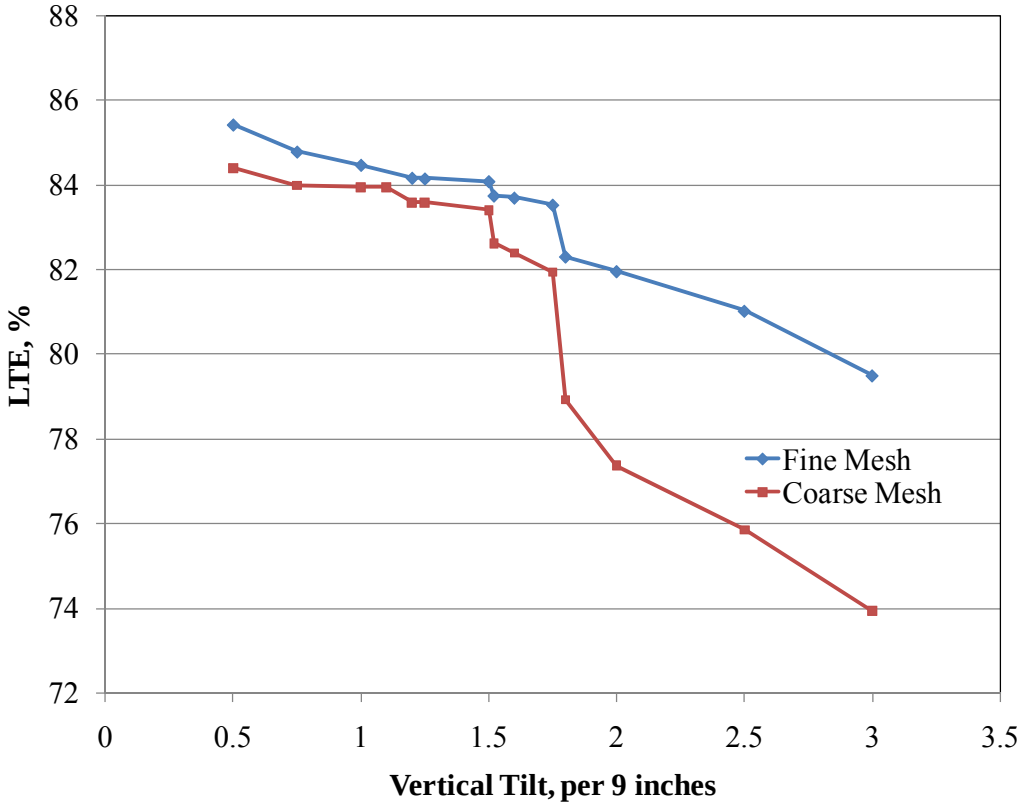

Figure D.31. Fine Mesh versus Coarse Mesh

D.8 RESULTS FROM FINITE ELEMENT ANALYSIS OF THE SLAB MODEL

There is a concern that dowel misalignment may increase longitudinal tensile stresses in the concrete slab due to higher dowel resistance to joint opening (joint lockup). If these longitudinal stresses are sufficiently high, they may increase a potential of transverse cracking. To evaluate this phenomenon, the development of longitudinal stresses in concrete during the joint opening step was analyzed.

Figure D.32 presents the distribution of the longitudinal stresses at the top surface of the PCC slabs at the end of the joint opening step. The dowels in the joint are non-uniformly vertically tilted. One can observe from Figure D.32 that these stresses are not significant. This agrees with the results of the finite element and laboratory study conducted at Michigan State University (Prabhu et al., 2006). Although this study identified some difference in the pullout forces for aligned and misaligned dowels, the stresses caused by the misalignment were insignificant for joint openings as large as 0.5 in.

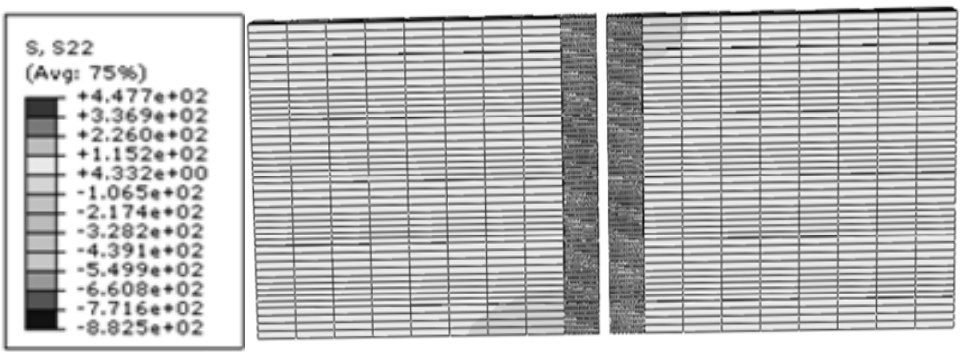

Figure D.32. Longitudinal stresses at the top surface of the PCC slab for non-uniformly vertically tilted dowels.

To evaluate the effect of dowel misalignment on the LTE, four combinations of vertical rotational misalignments were analyzed, as labeled in Figure D.33.

- Case 1: Each dowel rotated by the same amount, with the direction of rotation opposite for the adjacent dowels (Figure D.33a).
- Case 2: Each dowel tilted with the same magnitude and direction (Figure D.33b).
- Case 3: The dowel in the wheel path aligned properly, and each other dowel rotated with the same magnitude and direction (Figure D.33c).
- Case 4: The dowel at the wheel path rotated, and each other dowel aligned properly (Figure D.33d).

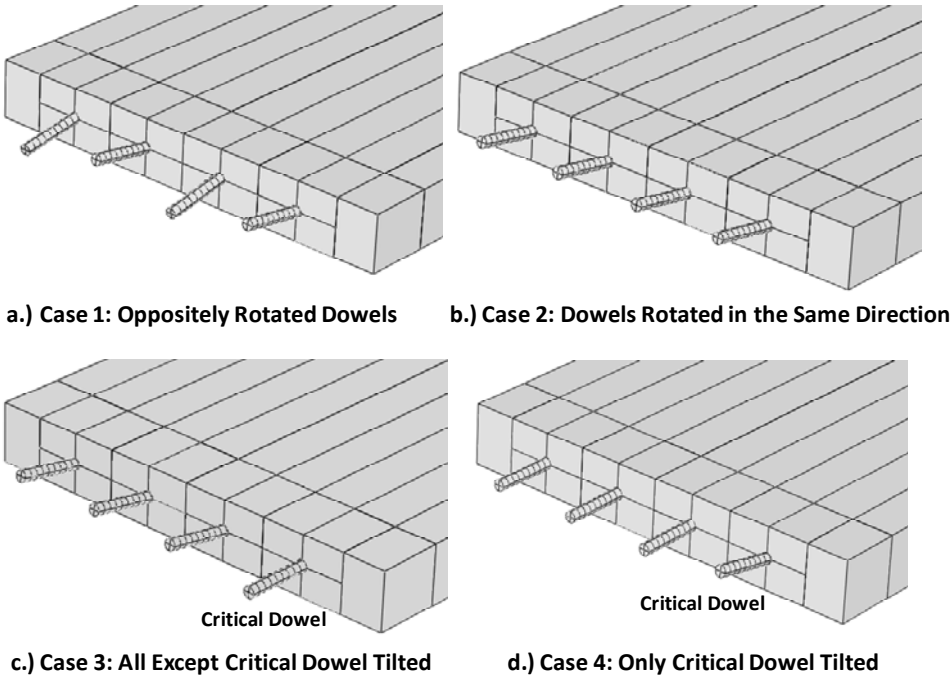

Figure D.33. Combinations of vertically rotated dowels.

LTE was determined for each case by dividing the unloaded corner deflection by the loaded slab corner deflections from the wheel load application as described in section 7.4

of the report. Table D.2 summarizes the considered combinations of dowel misalignment, calculated displacements of the loaded and unloaded slabs, and the resulting LTEs. The information obtained from this factorial of the ABAQUS runs was used to develop a predictive equation of the joint LTE for an arbitrary combination of dowel misalignments. First, for each combination of dowel misalignment, the non-dimensional joint stiffness was determined using the following equation (Khazanovich and Gotlif, 2002):

$$JStiff = \left(\frac{\frac{1}{LTE} - 0.01}{0.012} \right)^{-1.17786} \tag{D.2}$$

Where *JStiff* is the non-dimensional joint stiffness and LTE is expressed as a percentage. Linear regression analysis was used to develop the following relationship:

$$JStiff = JStiff_0 - 0.20623 \times MeanTilt - 0.61796 \times StDTilt - 0.86862 \times WPTilt \tag{D.3}$$

Statistics: $R^2 = 0.93$, SEE = 0.31, N = 26

Where *MeanTilt* is the average tilt of the dowels in the joint, *StDTilt* is the standard deviation of the tilt of the dowels in the joint, and *WPTilt* is the wheelpath dowel tilt. $JStiff_0$ is the predicted non-dimensional stiffness of the joint with aligned dowels. The value of $JStiff_0$ for each dowel diameter is presented in Table D.3.

Using this non-dimensional joint stiffness, the joint load transfer efficiency was predicted using the following equation (Crovetti, 1994):

$$LTE = \frac{100\%}{1 + 1.2 * (JStiff)^{-0.849}} \tag{D.4}$$

Equations D.3 and D.4 permit prediction of the joint load transfer efficiency in the finite element slab model for various dowel diameters and combinations of dowel misalignments. Table D.4 presents the computed mean dowel rotation, dowel rotation standard deviation, and critical dowel rotation, joint stiffness backcalculated from the ABAQUS LTE values, joint stiffness predicted from equation D.3, and LTE predicted from equation D.4. Figure 3.38 in the report presents the load transfer efficiencies predicted using equations D.3 and D.4 versus the load transfer efficiencies determined directly from the finite element slab model. These values were found to correlate well.

To further verify the predictive equations D.3 and D.4, several additional ABAQUS runs were made for the combinations of dowel rotational misalignment not included into the model development. First, six cases of non-uniform dowel misalignments were considered. The LTE from ABAQUS and the predictive equations were determined.

Table D.5 summarizes the results of this analysis. A good correspondence between two the LTEs is observed for all combinations of misalignments.

Given the LTE analysis for levels of misalignment, 17 combinations of dowel horizontal skews were considered. Table D.6 presents the considered combinations of dowel misalignment along ABAQUS corner deflections and computed LTEs. Figure D.34 presents the comparison between the LTEs for the ABAQUS simulations and the predictive equations D.3 and D.4. A very good correlation between these values is observed, confirming the robustness of the predictive model.

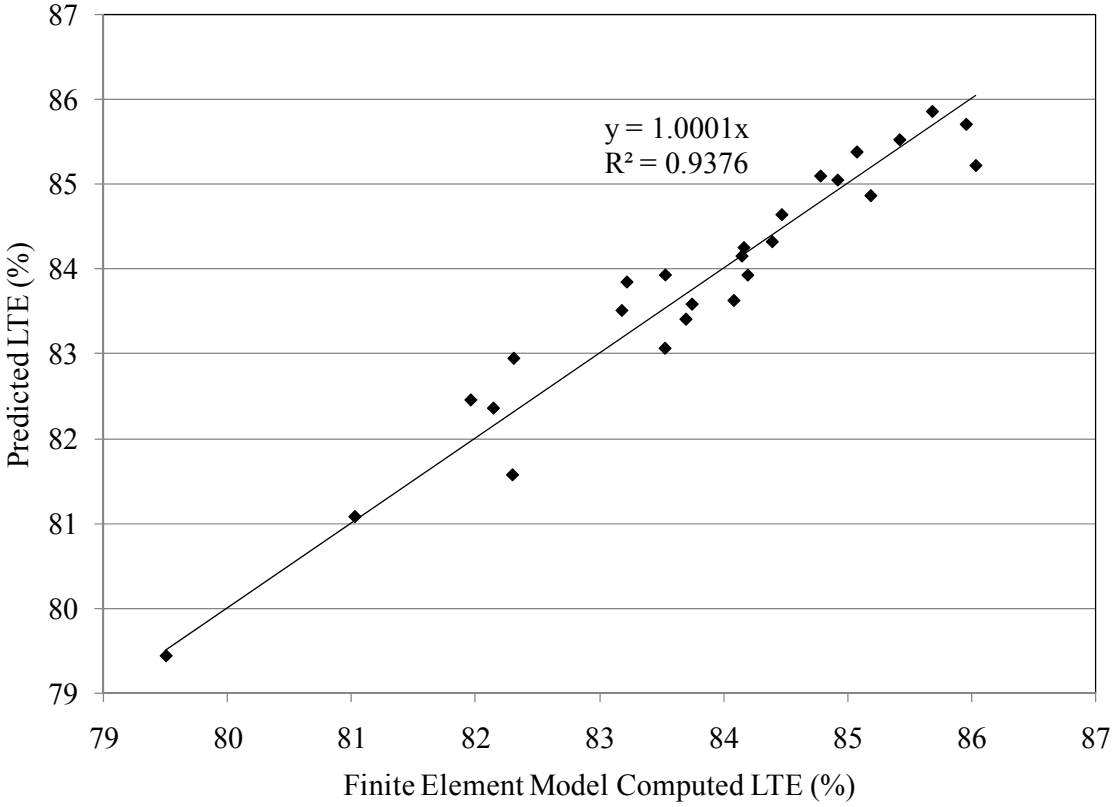

Figure D.34. Slab model versus regression predicted LTEs for various horizontal rotational misalignments.

Table D.2. Cases of dowel misalignment used for modeling ABAQUS slab model, displacements of the loaded and unloaded slabs, and LTEs.

Case Type	Dowel Diameter (in)	Rotation Magnitude (in/18in)	Deflection		Model LTE %
			Loaded ΔL (in)	Unloaded ΔU (in)	
Case 1	1.5	0.5	0.02722	0.02326	85.42011
Case 1	1.5	0.75	0.02737	0.02321	84.78154
Case 1	1.5	1	0.02746	0.02320	84.46901
Case 1	1.5	1.2	0.02755	0.02318	84.16312
Case 1	1.5	1.25	0.02755	0.02318	84.14716
Case 1	1.5	1.5	0.02759	0.02320	84.08206
Case 1	1.5	1.52	0.02764	0.02315	83.74456
Case 1	1.5	1.6	0.02765	0.02314	83.69506
Case 1	1.5	1.75	0.02769	0.02313	83.52644
Case 1	1.5	1.8	0.02797	0.02302	82.30618
Case 1	1.5	2	0.02800	0.02295	81.95927
Case 1	1.5	2.5	0.02815	0.02281	81.02428
Case 1	1.5	3	0.02839	0.02257	79.50119
Case 2	1.5	1	0.02714	0.02335	86.03449
Case 2	1.5	2	0.02762	0.02307	83.52914
Case 2	1.5	3	0.02783	0.02286	82.14201
Case 3	1.5	1	0.02716	0.02327	85.68346
Case 3	1.5	2	0.02729	0.02322	85.0752
Case 3	1.5	3	0.02734	0.02329	85.18659
Case 4	1.5	0.5	0.02711	0.02330	85.95672
Case 4	1.5	1	0.02727	0.02316	84.91945

Case Type	Dowel Diameter (in)	Rotation Magnitude (in/18in)	Deflection		Model LTE %
			Loaded ΔL (in)	Unloaded ΔU (in)	
Case 4	1.5	1.5	0.02737	0.02310	84.39172
Case 4	1.5	1.75	0.02740	0.02307	84.1943
Case 4	1.5	1.8	0.02763	0.02300	83.21925
Case 4	1.5	2	0.02762	0.02297	83.17814
Case 4	1.5	3	0.02772	0.02281	82.29567
Case 1	1.25	0.5	0.02788	0.02305	82.69373
Case 1	1.25	0.75	0.02801	0.02296	81.97041
Case 1	1.25	1	0.02811	0.02292	81.54157
Case 1	1.25	1.25	0.02815	0.02292	81.42342
Case 1	1.25	1.5	0.02824	0.02288	81.03107
Case 1	1.25	1.56	0.02825	0.02288	80.97316
Case 1	1.25	1.58	0.02831	0.02281	80.55495
Case 1	1.25	1.75	0.02833	0.02280	80.47555
Case 1	1.25	2	0.02868	0.02259	78.76044
Case 1	1.25	2.5	0.02877	0.02250	78.19703
Case 1	1.25	3	0.02899	0.02227	76.80279
Case 2	1.25	1	0.02778	0.02318	83.46088
Case 2	1.25	2	0.02838	0.02276	80.19507
Case 2	1.25	3	0.02861	0.02252	78.71879
Case 3	1.25	1	0.02780	0.02309	83.06475
Case 3	1.25	2	0.02796	0.02300	82.27521
Case 3	1.25	3	0.02800	0.02303	82.25221
Case 4	1.25	0.5	0.02775	0.02314	83.36252
Case 4	1.25	1	0.02791	0.02299	82.38943

Case Type	Dowel Diameter (in)	Rotation Magnitude (in/18in)	Deflection		Model LTE %
			Loaded ΔL (in)	Unloaded ΔU (in)	
Case 4	1.25	1.5	0.02800	0.02294	81.9235
Case 4	1.25	2	0.02831	0.02273	80.27591
Case 4	1.25	3	0.02837	0.02264	79.80853

Table D.3. Predicted non-dimensional stiffness ($JStiff_0$) of the joint in the slab finite element model for various dowel diameters.

Dowel Diameter (in)	$JStiff_0$
1	6.537
1.125	7.447
1.25	8.461
1.375	9.601
1.5	10.894

Table D.4. Vertical tilt cases used for development of the LTE predictive equations.

Case Type	Dowel Diameter (in)	Rotation Magnitude (in/18in)	Mean Rotation (in/18in)	Standard Deviation (in/18in)	WP Dowel Rotation (in/18in)	Model LTE %	Model Joint Stiffness	Regression Joint Stiffness	Predicted LTE %
Case 1	1.5	0.5	0	0.5	0.5	85.42011	9.945633	10.1031133	85.58552
Case 1	1.5	0.75	0	0.75	0.75	84.78154	9.372732	9.70756688	85.16215
Case 1	1.5	1	0	1	1	84.46901	9.111259	9.31202049	84.71029
Case 1	1.5	1.2	0	1.2	1.2	84.16312	8.866366	8.99558339	84.32624
Case 1	1.5	1.25	0	1.25	1.25	84.14716	8.853875	8.91647411	84.22687
Case 1	1.5	1.5	0	1.5	1.5	84.08206	8.803211	8.52092773	83.7083
Case 1	1.5	1.52	0	1.52	1.52	83.74456	8.54774	8.48928402	83.66518
Case 1	1.5	1.6	0	1.6	1.6	83.69506	8.511249	8.36270917	83.49013

Case Type	Dowel Diameter (in)	Rotation Magnitude (in/18in)	Mean Rotation (in/18in)	Standard Deviation (in/18in)	WP Dowel Rotation (in/18in)	Model LTE %	Model Joint Stiffness	Regression Joint Stiffness	Predicted LTE %
Case 1	1.5	1.75	0	1.75	1.75	83.52644	8.388777	8.12538134	83.15044
Case 1	1.5	1.8	0	1.8	1.8	82.30618	7.579082	8.04627207	83.03375
Case 1	1.5	2	0	2	2	81.95927	7.370951	7.72983496	82.54846
Case 1	1.5	2.5	0	2.5	2.5	81.02428	6.851844	6.93874219	81.18832
Case 1	1.5	3	0	3	3	79.50119	6.117949	6.14764942	79.5682
Case 2	1.5	1	1	0	1	86.03449	10.55167	9.81935598	85.28456
Case 2	1.5	2	2	0	2	83.52914	8.39072	8.74450593	84.00596
Case 2	1.5	3	3	0	3	82.14201	7.479471	7.66965589	82.45266
Case 3	1.5	1	0.75	0.433013	0	85.68346	10.19837	10.4305536	85.91638
Case 3	1.5	2	1.5	0.866025	0	85.0752	9.62947	9.9669012	85.44276
Case 3	1.5	3	2.25	1.299038	0	85.18659	9.729793	9.50324879	84.93248
Case 4	1.5	0.5	0.125	0.216506	0.5	85.95672	10.47172	10.2796254	85.76598
Case 4	1.5	1	0.25	0.433013	1	84.91945	9.491928	9.66504476	85.11499
Case 4	1.5	1.5	0.375	0.649519	1.5	84.39172	9.048381	9.05046412	84.39437
Case 4	1.5	1.75	0.4375	0.757772	1.75	84.1943	8.890847	8.7431738	84.00422
Case 4	1.5	1.8	0.45	0.779423	1.8	83.21925	8.172647	8.68171574	83.92359
Case 4	1.5	2	0.5	0.866025	2	83.17814	8.144386	8.43588348	83.59183
Case 4	1.5	3	0.75	1.299038	3	82.29567	7.572645	7.20672221	81.67476
Case 1	1.25	0.5	0	0.5	0.5	82.69373	7.822547	7.66973304	82.45279
Case 1	1.25	0.75	0	0.75	0.75	81.97041	7.377497	7.27418666	81.79286
Case 1	1.25	1	0	1	1	81.54157	7.131832	6.87864028	81.07526
Case 1	1.25	1.25	0	1.25	1.25	81.42342	7.066357	6.48309389	80.29172
Case 1	1.25	1.5	0	1.5	1.5	81.03107	6.855409	6.08754751	79.43226
Case 1	1.25	1.56	0	1.56	1.56	80.97316	6.825085	5.99261638	79.2134

Case Type	Dowel Diameter (in)	Rotation Magnitude (in/18in)	Mean Rotation (in/18in)	Standard Deviation (in/18in)	WP Dowel Rotation (in/18in)	Model LTE %	Model Joint Stiffness	Regression Joint Stiffness	Predicted LTE %
Case 1	1.25	1.58	0	1.58	1.58	80.55495	6.612074	5.96097266	79.13929
Case 1	1.25	1.75	0	1.75	1.75	80.47555	6.572771	5.69200112	78.48474
Case 1	1.25	2	0	2	2	78.76044	5.803076	5.29645474	77.43421
Case 1	1.25	2.5	0	2.5	2.5	78.19703	5.579477	4.50536197	74.94444
Case 1	1.25	3	0	3	3	76.80279	5.077881	3.71426921	71.74243
Case 2	1.25	1	1	0	1	83.46088	8.341906	7.38597576	81.98489
Case 2	1.25	2	2	0	2	80.19507	6.436747	6.31112571	79.92804
Case 2	1.25	3	3	0	3	78.71879	5.786094	5.23627567	77.26423
Case 3	1.25	1	0.75	0.433013	0	83.06475	8.067224	7.9971734	82.96041
Case 3	1.25	2	1.5	0.866025	0	82.27521	7.560135	7.53352098	82.23159
Case 3	1.25	3	2.25	1.299038	0	82.25221	7.546111	7.06986857	81.42988
Case 4	1.25	0.5	0.125	0.216506	0.5	83.36252	8.272349	7.84624517	82.73053
Case 4	1.25	1	0.25	0.433013	1	82.38943	7.630377	7.23166454	81.71862
Case 4	1.25	1.5	0.375	0.649519	1.5	81.9235	7.349994	6.6170839	80.5651
Case 4	1.25	2	0.5	0.866025	2	80.27591	6.475512	6.00250326	79.23643
Case 4	1.25	3	0.75	1.299038	3	79.80853	6.256149	4.77334199	75.85424

Table D.5. Various combinations of vertically tilted dowels used to verify ABAQUS computed LTEs against predicted LTEs.

Case Type	Dowel Diameter (in)	Rotation Magnitude (in/18in)				Mean Rotation (in/18in)	Standard Deviation (in/18in)	WP Dowel Rotation (in/18in)	Regression Joint Stiffness	Model LTE %	Predicted LTE %
		Dowel 1 (critical)	Dowel 2	Dowel 3	Dowel 4						
Combo 1	1.5	2.0	2.0	-2.0	-2.0	0.00	2.00000	2.00	7.92084	82.19082	82.845
Combo 2	1.5	0.0	0.0	-3.0	3.0	0.00	2.12132	0.00	9.58311	86.85441	85.02318
Combo 3	1.5	2.0	2.0	2.0	0.0	1.50	0.86603	2.00	8.31225	83.89135	83.41917
Combo 4	1.5	2.0	-2.0	0.0	0.0	0.00	1.41421	2.00	8.28283	82.16053	83.37750
Combo 5	1.5	2.0	1.5	1.0	0.5	1.25	0.55902	2.00	8.55352	83.14311	83.75246
Combo 6	1.5	2.0	-1.5	1.0	-0.5	0.25	1.34629	2.00	8.27325	82.20433	83.36388

Table D.6. Various combinations of horizontally skewed dowels used to verify ABAQUS computed LTEs against predicted LTEs.

Case Type	Dowel Diameter (in)	Rotation Magnitude (in/18in)	Mean Rotation (in/18in)	Standard Deviation (in/18in)	WP Dowel Rotation (in/18in)	Regression Joint Stiffness	Model LTE %	Predicted LTE %
Case 1	1.5	0.50	0.00	0.5	0.50	10.15071	86.70644	85.63468
Case 1	1.5	1.00	0.00	1	1.00	9.40742	85.49865	84.82204
Case 1	1.5	1.50	0.00	1.5	1.50	8.66413	83.49201	83.90035
Case 1	1.5	2.00	0.00	2	2.00	7.92084	81.55764	82.84500
Case 1	1.5	3.00	0.00	3	3.00	6.43426	78.61538	80.18994
Case 2	1.5	1.00	0.00	1.00	1.00	9.40742	86.25354	84.82204
Case 2	1.5	2.00	0.00	2.00	2.00	7.92084	83.12856	82.84500
Case 2	1.5	3.00	0.00	3.00	3.00	6.43426	80.06468	80.18994
Case 3	1.5	1.00	0.75	0.43301	0.00	10.47174	87.00708	85.95682
Case 3	1.5	2.00	1.50	0.86603	0.00	10.04949	86.71950	85.52968
Case 3	1.5	3.00	2.25	1.29904	0.00	9.62723	86.53110	85.07277
Case 4	1.5	0.50	0.13	0.21651	0.50	10.30012	86.90848	85.78661
Case 4	1.5	1.00	0.25	0.43301	1.00	9.70624	85.85542	85.16068

Case Type	Dowel Diameter (in)	Rotation Magnitude (in/18in)	Mean Rotation (in/18in)	Standard Deviation (in/18in)	WP Dowel Rotation (in/18in)	Regression Joint Stiffness	Model LTE %	Predicted LTE %
Case 4	1.5	1.50	0.38	0.64952	1.50	9.11236	84.22878	84.47043
Case 4	1.5	2.00	0.50	0.86603	2.00	8.51848	82.69340	83.70497
Case 4	1.5	3.00	0.75	1.29904	3.00	7.33071	80.42527	81.89053

D.9 REFERENCES

ABAQUS/CAE User's Manual, version 6.7, Dassault Systemes, Providence, RI, 2007.

Crovetti, J.A. "Evaluation of Jointed Concrete Pavement Systems Incorporating Open-Graded Permeable Bases." Ph.D. Dissertation, University of Illinois at Urbana-Champaign, 1994.

Khazanovich, L., N. Buch, and A. Gotlif, "Mechanistic Evaluation of Vertical Misalignment of Dowel Bars and their Effect on Joint Performance," *Proceedings*, 7th International Conference on Concrete Pavement, Lake Buena Vista, FL, September 2001, pp. 525-538.

Lee, J., and G.L. Fenves, "Plastic-Damage Model for Cyclic Loading of Concrete Structures," *Journal of Engineering Mechanics*, Vol. 124, No.8, 1998, pp. 892–900.

Lubliner, J., J. Oliver, S. Oller, and E. Oñate, "A Plastic-Damage Model for Concrete," *International Journal of Solids and Structures*, Vol. 25, 1989, pp. 299–329.

Mindess, S., J.F. Young, and D. Darwin, *Concrete*, Pearson Education, Inc., Upper Saddle River, NJ, 2003.

Prabhu M., N. Buch, A.H. Varma, and D. Thandaveswara, "Experimental Investigation of the Effects of Dowel Misalignment on Joint Opening Behavior in Rigid Pavements," *Transportation Research Board No. 1947*, Transportation Research Board of the National Academies, Washington, DC, 2006.